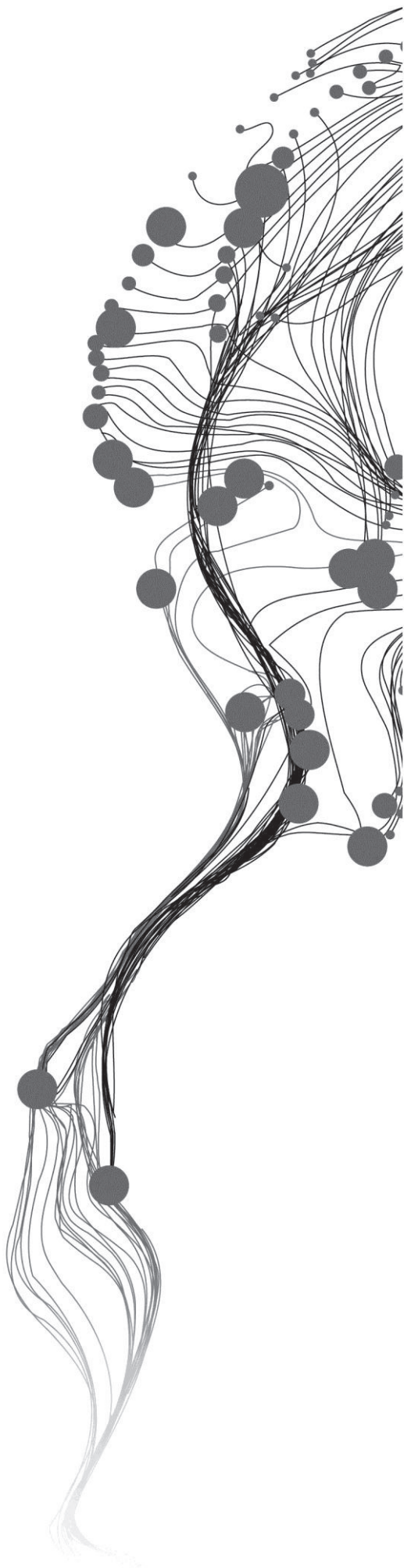


# Polarimetric scattering model for biophysical characterization of multilayer vegetation using space borne PolSAR data

SAI BHARADWAJ POOLLA  
March, 2013

SUPERVISORS:  
Mr. Shashi Kumar  
Dr. S.P.S. Kushwaha  
Dr. ir. Wietske Bijker



# Polarimetric scattering model for biophysical characterization of multilayer vegetation using space borne PolSAR data

SAI BHARADWAJ POOLLA

Enschede, The Netherlands, March, 2013

Thesis submitted to the Faculty of Geo-Information Science and Earth Observation of the University of Twente in partial fulfilment of the requirements for the degree of Master of Science in Geo-information Science and Earth Observation.  
Specialization: Geoinformatics

## **SUPERVISORS**

Mr. Shashi Kumar

Dr. S.P.S. Kushwaha

Dr. ir. Wietske Bijker

## **THESIS ASSESSMENT BOARD**

Chairperson : Professor George Vosselman

ITC Professor : Professor Alfred Stein

IIRS supervisor : Mr. Shashi Kumar

IIRS supervisor : Dr.S.P.S. Kushwaha

ITC supervisor : Dr. ir. Wietske Bijker

External examiner : Mr. Sanjay (DEAL, Dehradun)

## **DISCLAIMER**

This document describes work undertaken as part of a programme of study at the International Institute for Geo-information Science and Earth Observation. All views and opinions expressed therein remain the sole responsibility of the author, and do not necessarily represent those of the institute.

*Dedicated to my family*



## ABSTRACT

Forests are the important biomes covering major part of the vegetation on the Earth and accounts for 70 percent of the carbon present in the living beings. Due to deforestation and conversion of forest land for cultivation resulted in decrease of area under forests cover. Stem volume and AGB are considered as parameters in assessing the quality of the forests and in turn assessing the carbon content. Forests with vast coverage and varied variety of species make the *in-situ* management and monitoring of forests a tedious and labour intensive task. The remote sensing due to its high repetitive coverage and wide swath is considered to be an efficient tool for the monitoring of the forest parameters and change in the forest cover. Remote sensing in the microwave region of the electromagnetic spectrum has the advantage of all-weather capability and penetration through cloud cover and canopy, makes it suitable for the monitoring of the forests. Previous studies have shown the potential of polarimetric SAR in assessing the forest parameters like stem volume and AGB, but the need for a standardized approach still exists. For this study ALOS-PALSAR full polarimetric L-band data is used for the estimation stem volume and AGB in the Dudhwa National Park area. The present study aims at developing a polarimetric scattering model for the estimation of stem volume and AGB using quad-pol L-band data of ALOS-PALSAR in Dudhwa National Park area. Previous research has shown that the PolSAR data is affected by the orientation angle (OA) shifts and compensating these OA shifts (deorientation) effect the polarimetric decomposition components like volume scattering, double bounce scattering and surface scattering and this effect of OA shifts are considered in the present study. The previously developed semi-empirical models like water cloud model (WCM) does not consider the higher order scattering mechanisms like double scattering from the ground stem interactions. The higher order scattering mechanisms which are prominent in longer wavelengths are considered in the present study for the modelling of stem volume and AGB by extending the water cloud model for ground stem interactions. The parameters of the extended water cloud model are estimated using the decomposition components and the *in-situ* measurements of selected plots. The stem volume and AGB are modelled and accuracy is assessed for the remaining plots which are not used in the parameter estimation. The results showed a consistent effect orientation angle shift on the modelled stem volume and AGB. The stem volume and AGB has shown better correlation and low root mean square error with respect to the field estimated stem volume and AGB respectively when deorientation is applied.

**Key words:** PALSAR, orientation angle, polarimetric decomposition, above ground biomass, stem volume, semi-empirical modelling.

## ACKNOWLEDGEMENTS

I am thankful to my IIRS supervisor, Mr. Shashi Kumar sir, for his constant support and guidance. His interest, patience and care in supporting me can never be valued. He was always available with his valuable suggestions whenever I need his guidance and support throughout my research work. I would always consider him as my motivation and inspiration without whom this thesis would have been a distant dream.

I am thankful to my IIRS supervisor, Dr. S.P.S. Kushwaha sir, for his motivation and guidance throughout my research. His guidance has not only helped me in my research but also helped me in improvising myself personally.

I am greatly thankful to my ITC supervisor, Dr. ir. Wietske Bijker madam. Her support and guidance, throughout my research work, helped me in completing my thesis in time. Her valuable and detailed suggestions helped me to carry out my research in the best possible manner.

“Pace and quality in work”, “Efficient management of time and resources in work”, “Analysing in an innovative and critical manner” are the three important points I have observed and learnt from my supervisors. I would put every effort to implement these qualities in every step of my life. It is my privilege to work under such knowledgeable supervision.

I also thank Dr. Nicolas Hamm sir for his arrangements and care through of out the course and during our stay in ITC.

I also thank Mr. P.L.N. Raju sir, and Dr. S.K. Srivastav sir for their enduring support and assurance during the entire course period. I thank the CMA department for the technical support extended throughout the course.

I am greatly thankful to the Director, IIRS, Dr. Y.V.N. Krishnamurthy sir and former Director, Dr. P.S. Roy for creating an environment for better research at IIRS.

I am greatly obliged to my parents Mr. P. V. Subba Rao and Mrs. Ganga Bhavani, without whom, all this would never been possible. They have encouraged me in all my endeavours and supported me in all ways and means. I also thank my loving sister Ms. P. Sirisha Tushara, who is always available for me in my good and bad times. My parents and sister are my greatest source of my inspiration.

I am thankful to all the staff at IIRS and ITC for making my stay in IIRS and ITC a memorable one.

Last but not the least, my friends also need a special mention here. I thank my friends Shankar, Pavan, Bhavya, Pavan Kumar, Hemanth, Ankur, Jayson, Ravi, Mrinal, Sarath, Chetan, Deepak, Dipima, Anukesh, Sruthi, Balaji sir, Anudeep, Vineet, my seniors Teja, Vishnu, Verma, Abhishek, my juniors Akhil, Abhishek for all the support and help I received from them throughout the duration of my course at IIRS and ITC.

# TABLE OF CONTENTS

---

1. INTRODUCTION:.....	1
1.1. Radar remote sensing:.....	1
1.2. Polarization and SAR polarimetry:.....	2
1.3. Motivation and Problem statement: .....	3
1.4. Research Identification: .....	4
1.4.1. Research objectives: .....	4
1.4.2. Sub objectives:.....	4
1.4.3. Research Questions:.....	4
2. LITERATURE REVIEW.....	5
2.1. Radar remote sensing:.....	5
2.1.1. SAR polarimetry: .....	6
2.1.2. Scattering matrix, covariance matrix, coherency matrix: .....	6
2.2. Orientation angle shifts:.....	8
2.3. Polarimetric decompositions:.....	10
2.4. Methods of estimating forest biophysical parameters:.....	11
2.4.1. Field measurements:.....	11
3. Study area: .....	17
3.1. Significance of the study area:.....	17
4. Materials and Methods .....	19
4.1. Dataset description:.....	19
4.2. Forest inventory data collection: .....	20
4.3. Methodology Flow Chart: .....	21
4.4. Methodology:.....	22
4.4.1. Data pre-processing: .....	22
4.4.2. Coherency matrix generation from the scattering matrix:.....	23
4.4.3. Decomposition of Coherency matrix:.....	23
4.4.4. Calculation of OA shift using coherency matrix:.....	26
4.4.5. Decomposition of the coherency matrix after deorientation:.....	27
5. Modelling approach: Water Cloud Model and Extended Water cloud model .....	29
5.1. Water Cloud Model (WCM):.....	29
5.2. Extended Water cloud model (WCM) for higher order interactions:.....	31
5.2.1. Backscattering from the ground-stem interaction from the canopy gaps:.....	31
5.2.2. Backscattering from the stem ground interaction through the canopy:.....	32

5.3.	Using polarimetric SAR for extended water cloud modelling:.....	33
6.	Results and discussions:.....	35
6.1.	Orientation angle shift:.....	35
6.2.	Effect of OA shift compensation on the decomposition components:.....	36
6.2.1.	Volume scattering:.....	36
6.2.2.	Double-bounce scattering:.....	38
6.2.3.	Surface scattering:.....	38
6.3.	Extended Water cloud model parameter estimation and results:.....	39
6.3.1.	Parameter estimation of extended water cloud model using PolSAR data:.....	39
6.3.2.	Retrieval of $\beta$ for stem volume:.....	40
6.4.	Retrieval of stem volume:.....	41
6.5.	Modeling of AGB from PolSAR data:.....	44
6.5.1.	Retrieval of $\beta$ for AGB:.....	44
6.5.2.	Retrieval of AGB:.....	45
6.6.	Discussions:.....	48
7.	Conclusions and recommendations:.....	51
7.1	Conclusions:.....	51
7.2	Recommendations:.....	53
	REFERENCES.....	55

## LIST OF FIGURES

---

Figure 2-1 : Relation of radar geometry and planes ( source : Lee <i>et al</i> [24] ).....	8
Figure 2-2: Surface, Double-bounce and Volume scattering.....	9
Figure 3-1 : Figure 1 : PolSAR data foot print shown on the Google Earth image with location in India ( Source : India and Uttar Pradesh images from S Kumar [19] and Google Earth image of 22 <sup>nd</sup> Feb 2012) .....	18
Figure 4-1 : ETM+ FCC imaging showing the <i>in-situ</i> data collected in the Dudhwa National Park.....	20
Figure 4-2 : Methodology Flow-chart .....	21
Figure 4-3 Pauli colour coded SAR images in SLC format and Multilooked image with HH-VV, HV, HH+VV in Red, Green and Blue bands respectively.....	22
Figure 4-4 : Decomposition components shown in RGB. Red - double-bounce (DBL), Green - Volume scattering (VOL), Blue - Odd bounce or Surface scattering (ODD).....	26
Figure 4-5 : Decomposition components obtained after deorientation displayed in RGB. Red-Double-bounce (DBL), Green-Volume scattering (VOL), Blue-surface scattering (ODD) ....	27
Figure 5-1 : Water Cloud Model showing backscattering from canopy $\sigma_{veg}^{\circ}$ and backscattering from ground $\sigma_{gr}^{\circ}$ .....	30
Figure 5-2 : Ground-Stem interaction $\sigma_{gs}^{\circ}$ from canopy gaps.....	31
Figure 5-3 : Ground-Stem interaction $\sigma_{gs}^{\circ}$ through canopy .....	32
Figure 6-1 : (a) Estimated orientation angle shift image and (b) Histogram of the image .....	35
Figure 6-2 : Images showing the volume scattering components before and after deorientation. Left and right images are before and after compensation results of volume scattering respectively .....	36
Figure 6-3 : ETM+ FCC image showing the plots selected for the analysis.....	37
Figure 6-4 : Volume scattering before and after deorientation .....	37
Figure 6-5 : Double-bounce scattering before and after deorientation.....	38
Figure 6-6 : Surface scattering before and after deorientation .....	39
Figure 6-7 : Plot showing the relationship between the field estimated stem volume and the modelled stem volume (a) before deorientation (b) after deorientation .....	42
Figure 6-8 : Plot showing the relationship between the field estimated AGB and the modelled AGB (a) before deorientation (b) after deorientation.....	46

## LIST OF TABLES

---

Table 2-1: Radar bands and their wavelengths as in [6] .....	5
Table 4-1: Data characteristics .....	19
Table 4-2 : stratum wise number of clusters and plots.....	20
Table 6-1: Estimated $\beta_v$ values for the modelling of stem volume.....	41
Table 6-2 : $\beta$ , RMSE and R-square obtained for modelled stem volume before and after deorientation.....	43
Table 6-3 : RMSE obtained for the plots with field estimated stem volume < 300 m <sup>3</sup> /ha.....	43
Table 6-4 : Estimated $\beta_B$ values for the modelling of AGB.....	45
Table 6-5: $\beta$ , RMSE and R-square obtained for modelled AGB before and after deorientation .....	47
Table 6-6 : RMSE obtained for the plots with field estimated AGB < 300 tons/ha .....	47

## 1. INTRODUCTION:

Forests make major part of the vegetation on the Earth. About one-third of the Earth's land area is covered by forests and accounts for major carbon present in the living beings [1] [2]. Forests role in the conservation of ecosystem is of high magnitude. The severity of floods, avalanches and draughts can be reduced to a greater extent by the forests. Forests, however, are being influenced by the changing temperature and precipitation pattern and increasing concentrations of CO<sub>2</sub> in the atmosphere [3]. Forests ameliorate climate by maintaining the quantity of carbon dioxide in the atmosphere.

The history of human existence is entwined with forests and trees, and the use of the forest products by human's dates back to the human occupation on this Earth. The ever increasing human population and need for settling and agricultural are one of the important reasons for the thinning of forest cover. The exploitation of forests for fuel and other products resulted in the decrease of forests cover. The conversion of forests in to agricultural land is happening at alarming rate. Forests are home for more than 300 M people around the world [1]. FAO reports an annual total of decline in the forests at the rate of 13 M hectares across the globe in the last decade [1]. These show the need for altruistic behaviour of humans by protecting and monitoring our forests for next generations. The dependency of human on the forests for food, fuel and economy leads to the need for continuous monitoring of forests.

The forest inventory measurements are important for the monitoring of forests. The quality as well as the cover of the forest is assessed by these measurements. Biomass is the organic matter produced by the plants by the process of photosynthesis in which sunlight is stored in the form of chemical energy; stem volume is the volume of the stem, down to a given diameter, excluding the branches and stumps [4] and biomass is defined as the amount organic matter present in the vegetation and all the biomass above soil is called AGB [5]. Biomass and stem volume which are obtained from the forest inventory measurements are considered for the assessment of the forest quality. Biomass is an essential variable in assessing the changes in the carbon cycle and in the modelling of carbon in the ecosystems [4] and estimates of the biomass are of extreme importance for the global carbon assessment. Remote sensing is already proven to be an efficient tool in monitoring the forests and estimation of the forest parameters like Above Ground Biomass (AGB), average tree height, basal area, stem volume (SV). The potential of optical remote sensing is limited to the visibility of the canopy, cloud cover, haze and whereas the microwaves due to their longer wavelengths (L-band 15-20 cm) can provide the information about the canopy, stem and ground also.

### 1.1. Radar remote sensing:

RADAR stands for **R**adio **D**etection and **R**anging. Radar remote sensing utilizes the microwave region of wavelength 1mm to 1.3m of the electromagnetic (EM) spectrum [6]. Active radar

system generates its own radar pulse for the illumination of the target and reduces its limitation of its use only in the night. Radar is a ranging instrument which transmits the microwave signal towards the target and detects the backscatter radiation and the time delay between the transmitted signal and the received signal along with the strength of the returned signal is used to characterize the target [6].

The radar backscatter is dependent on the physical properties of the target like area, shape, dielectric constant, moisture, etc., unlike other remote sensing instruments working in the visible spectrum measuring the reflectance from the targets[7]. The advent of side looking radar systems like SAR, high resolutions are obtained by synthesizing the antenna length, as the resolution is proportional to the antenna length and so the more precise measure of physical properties of targets. These unique features of the radar remote sensing are helpful in monitoring the physical properties of trees and can be related to the biomass and stem volume of the forests [8].

## 1.2. Polarization and SAR polarimetry:

Polarization is an important characteristic of EM wave that influence the transmission characteristics of the SAR system [7]. Polarization describes the orientation of the electric field plane with the plane orthogonal to its plane of propagation; it can be horizontal, vertical or at any angle and polarimetry is to describe the polarization properties of the radar wave. Synthetic Aperture Radar is an active side looking imaging radar system on a moving platform and the introduction of SAR system has achieved greater azimuthal resolutions using small antennas [7]. The long antenna is realized electronically by synthesizing the antenna length using Doppler principles [7].

Complex SAR systems are designed to transmit and receive polarizations like Horizontal (H) and Vertical (V).

- Horizontal transmit and Horizontal receive – HH
- Vertical transmit and Vertical receive – VV
- Horizontal transmit and Vertical receive – HV
- Vertical transmit and horizontal receive – VH

HH, VV represents co-polarized channels and HV, VH represents cross-polarized channels. The SAR systems which can transmit and receive either HH or VV or HV or VV are called single polarized, dual – polarized are those which can receive HH and VV or HH and HV or VV and VH [9]. The systems which can transmit and receive all the four polarizations are called Quad-polarized systems [9]. The SAR illuminated target, scatters the incident wave in all possible directions and the backscatter wave contains the information related to the physical properties of the target. The SAR illuminated target may affect the polarization of the incident wave and this backscattering information is used to identify different scattering mechanisms exhibited by the different targets.

### 1.3. Motivation and Problem statement:

Polarimetric decomposition theorems have been developed for the better interpretation of the targets, by considering the different scattering mechanisms that occur on the ground; incoherent target decompositions based on second order descriptors of the scattering matrix like covariance and coherency matrixes are introduced for better interpretation of natural and distributed targets [10]. Coherency matrix and covariance matrix are obtained from the vector form of the scattering matrix, which is generated using Pauli's and lexicographic representation [7]. Incoherent decomposition model have been developed for retrieving individual scattering mechanisms like volume scattering, surface scattering and double bounce scattering by Freeman *et al.* [11] considering the reflection symmetry and later helix scattering component was introduced in the decomposition by Yamaguchi *et al.* [12] by considering the non-reflection symmetry.

The orientation angle (OA) and the ellipticity describe the polarization state of the electromagnetic wave. The radar look angle and variations of terrain in azimuth and range directions may cause the shifts in the polarization OA. The shift in the OA is zero for reflection symmetry media like horizontal surfaces and there will be a shift in the OA for a non-horizontal medium [13]. These OA shifts results in the increase of cross-polarization intensity and this leads to increase in the volume scattering [13]. For the estimation of forest parameters like AGB and SV from the PolSAR data, these shifts affect the estimates due to the increase in volume scattering power and decrease in the double-bounce power. The OA shifts compensation (deorientation) has to be done on the backscatter for the accurate assessment of forest biophysical parameters from the PolSAR data.

For the estimation of bio-physical parameters of the forest like SV and AGB; semi-empirical models like water cloud model (WCM) [14], Michigan Microwave canopy scattering model (MIMICS) [15] have been developed. The behaviour of the radar backscatter with the forest parameters is explained by the WCM; which assumes the vegetation canopy as homogenous cloud and the vegetation matter as water particles over a horizontal surface which is considered as ground [14]. In the water cloud model the forest backscatter is expected to have contributions from the upper surface and from the ground with the energy attenuated during the transmission through layers. The higher order scattering mechanisms like ground stem interaction are not considered; which are not negligible at longer wavelengths [8].

A model similar to WCM which includes the scattering through the gaps in the canopy has been used for the estimation of the stem volume and biomass in the previous studies [16] [17]. Relating and retrieving SV and AGB from the PolSAR data using the semi-empirical modelling approach are shown in previous studies [18] [19][4]. Studies have been carried out to retrieve the SV and AGB using L-band fully polarimetric data and using model based decompositions [20][21]. Previous studies carried out for the retrieval of AGB and stem volume using semi-empirical modelling did not consider the higher order interactions. The effect of OA shift

compensation on the retrieved stem volume and AGB derived from the PolSAR data are yet to be studied.

This research is aimed at retrieving the forest biophysical parameters like stem volume and AGB using a semi-empirical water cloud model extended for higher order scattering mechanisms like ground stem interactions using the OA compensated PolSAR data decomposition components. This kind of study could be useful for the accurate assessment of the biophysical parameters using SAR data and for the regular monitoring of forests where traditional ground survey methods are tedious and accessibility is difficult.

## **1.4. Research Identification:**

### **1.4.1. Research objectives:**

The prime focus of this study is to explore the potential of fully polarimetric SAR in characterizing the biophysical parameters by assessing the effect of OA shift compensation on the decomposition components and the semi-empirical water cloud model extended for higher order scattering mechanisms.

### **1.4.2. Sub objectives:**

The following are the identified sub objectives to achieve the prime objective of this study.

- a) To identify the polarimetric scattering mechanisms sensitive to AGB and SV.
- b) To study the effect of the orientation angle shift compensation on decomposition components.
- c) Include higher order scattering mechanisms from ground stem interactions to WCM.
- d) To study the effect of the OA compensation on the estimated biomass and stem volume.
- e) Retrieve semi-empirical WCM parameters.
- f) To assess the accuracy of the modelled SV and AGB.

### **1.4.3. Research Questions:**

- a) Which scattering mechanism is better related to the field estimated stem volume and AGB?
- b) What is the effect of deorientation on the decomposition components?
- c) How can the WCM be extended to include higher order interactions?
- d) How can the parameters of the extended water cloud model be retrieved?
- e) How does the deorientation affect the estimated SV and AGB?
- f) What is the improvement in the results of model estimated AGB and SV before and after the OA compensation?
- g) What could be the accuracy of the modelled SV and AGB with respect to field estimated AGB and SV?

## 2. LITERATURE REVIEW

### 2.1. Radar remote sensing:

**R**adio **D**etection and **R**anging remote sensing utilizes the microwave region of wavelength 1 mm to 1.3 M of the electromagnetic (EM) spectrum [6]. Active radar system generates its own radar pulse for the illumination of the target and can therefore be used day and night. Radar is a ranging instrument which transmits the microwave signal towards the target and detects the backscatter radiation. The time delay between the transmitted signal and the received signal is used to measure the distance of the target from the antenna, and the strength of the received signal is used to characterize the target [6]. The transmitted and received energy are related by the radar equation which determines the amount of transmitted energy returned from the target [7].

$$P_r = \frac{P_t A^2 \sigma}{4\pi \lambda^2 R^4} \quad (2-1)$$

Here,  $P_r$  is the received power,  $P_t$  is the transmitted power,  $R$  is the distance from antenna to the target,  $\sigma$  is the scattering coefficient,  $A$  is the aperture of the receiving antenna and  $\lambda$  is the radar wavelength. The radar backscatter is dependent of different parameters like system parameters and target parameters. The system parameters are radar frequency, wavelength, polarization, look angle and resolution. The target parameters are area, shape, dielectric constant, moisture. Wavelength and polarization are important parameters of the radar system on which the backscattering properties are dependent. The radar wavelength increases, the penetration of the microwaves through canopy also increases. The Table 2-1 gives the details of the radar bands and their wavelength ranges used for radar remote sensing.

Table 2-1: Radar bands and their wavelengths as in [6]

Radar band	Wavelength in cm
Ka	0.75 – 1.10
K	1.10 – 1.67
Ku	1.67 – 2.40
X	2.40 – 3.75
C	3.75 – 7.50
S	7.50 – 15.0
L	15.0 – 30.0
P	30.0 – 130.0

### 2.1.1. SAR polarimetry:

Synthetic Aperture Radar is an active side looking imaging radar system on a moving platform, that synthesis longer antenna using Doppler principles [6] [7] . With the advent of SAR, high resolutions are obtained by synthesizing the antenna length, as the resolution is proportional to the antenna length and so the more precise measure of physical properties of targets. The introduction SAR system has achieved greater azimuthal resolutions using small antennas. The long antenna is realized electronically by synthesizing the antenna length using Doppler principles [7].

Polarization is an important characteristic of EM wave that influences the transmission characteristics of the SAR system. Polarization describes the orientation of the electric field plane with the plane orthogonal to its plane of propagation; it can be horizontal, vertical or at any angle; Polarimetry is to describe the polarization properties of the radar wave. The electric field and the magnetic field are always orthogonal to each other and perpendicular to the plane of propagation. Complex SAR systems are designed to transmit and receive polarizations like Horizontal (H) and Vertical (V).

- Horizontal transmit and Horizontal receive – HH
- Vertical transmit and Vertical receive – VV
- Horizontal transmit and Vertical receive – HV
- Vertical transmit and horizontal receive – VH

The SAR systems which can transmit and receive either HH or VV or HV or VV are called single polarized, dual – polarized systems are those which can receive HH and VV or HH and HV or VV and VH and the systems which can transmit and transmit all the polarizations are called Quad- polarized[9] [1].

### 2.1.2. Scattering matrix, covariance matrix, coherency matrix:

The SAR illuminated target, scatters the incident wave in all possible directions. In linear basis radar system transmits both horizontal and vertical wave and measures the polarization of the return signal [7]. The electric fields  $E_i$  and  $E_s$  of the incident wave and scattered wave respectively are related by a complex  $2 \times 2$  matrix called scattering matrix  $[S]$  [22], which contains the backscattering information of the target at each pixel for all the polarizations. They are related as

$$\begin{pmatrix} E_h^s \\ E_v^s \end{pmatrix} = \begin{pmatrix} S_{hh} & S_{hv} \\ S_{vh} & S_{vv} \end{pmatrix} \begin{pmatrix} E_h^i \\ E_v^i \end{pmatrix} \quad (2-2)$$

Each element of the scattering matrix is a measure of phase and amplitude of transmit and received wave in complex numbers [22]. The diagonal elements of the scattering matrix are called co-polarized i.e., they have the measurements of same transmit and receive polarizations. The off diagonal elements are called cross-polarized as they transmit one polarization and receive the

other. In the case of monostatic radars, the transmitter and receiver antenna are same unlike bistatic radars. In that case radar reciprocity is assumed which means the cross-polarized channels are same and symmetric [7] i.e.,  $S_{vh} = S_{hv}$ . The three independent complex measurements of the scattering matrix i.e., two co-polarised and one cross-polarized components are used to define a target vector  $K$  [6] [7][23], which is

$$k = V(S) = \frac{1}{2} \text{Tr}(S\psi) \quad (2-3)$$

Where  $S$  is the scattering matrix and  $\psi$  is the complete set of  $2 \times 2$  basis matrices which are orthogonal under Hermitian inner product. Targets in the environment are subjected to dynamical changes both spatially and temporally. These are called distributed targets. In order to describe the distributed targets second order statics of scattering matrix – coherency matrix and covariance matrix were introduced [23]. The  $4 \times 4$  coherency matrix and the  $4 \times 4$  covariance matrix are obtained from the Pauli's and lexicographic representations for the scattering target vector respectively [23] [9]. For monostatic backscattering, which considers reciprocity i.e.,  $S_{vh} = S_{hv}$  the lexicographic target vector which is obtained from the lexicographic matrix basis set, and they are as given in [23]

$$\varphi_L = \left\{ 2 \begin{bmatrix} 1 & 0 \\ 0 & 0 \end{bmatrix} \quad 2\sqrt{2} \begin{bmatrix} 0 & 1 \\ 0 & 0 \end{bmatrix} \quad 2 \begin{bmatrix} 0 & 0 \\ 0 & 1 \end{bmatrix} \right\} \quad (2-4)$$

And the corresponding the lexicographic target vector is represented as and the covariance matrix is obtained multiplying the lexicographic target vector with its complex conjugate.

$$k_L = \begin{bmatrix} S_{hh} \\ \sqrt{2} S_{hv} \\ S_{vv} \end{bmatrix} \quad (2-5)$$

$$\text{Covariance matrix } [C] = k_L k_L^\dagger = \begin{pmatrix} S_{hh} S_{hh}^* & \sqrt{2} S_{hh} S_{hv}^* & S_{hv} S_{vv}^* \\ \sqrt{2} S_{hv} S_{hh}^* & 2 S_{hv} S_{hv}^* & \sqrt{2} S_{hv} S_{vv}^* \\ S_{vv} S_{hh}^* & \sqrt{2} S_{vv} S_{hv}^* & S_{vv} S_{vv}^* \end{pmatrix} \quad (2-6)$$

Similarly, the coherency matrix  $[T]$  is generated from the vectorized form of the scattering matrix using Pauli's spin basis  $k_p$  and they are given as in [23]

$$\varphi_p = \left\{ \sqrt{2} \begin{bmatrix} 1 & 0 \\ 0 & 1 \end{bmatrix} \quad \sqrt{2} \begin{bmatrix} 1 & 0 \\ 0 & -1 \end{bmatrix} \quad \sqrt{2} \begin{bmatrix} 0 & 1 \\ 1 & 0 \end{bmatrix} \right\} \quad (2-7)$$

The coherency matrix is generated by multiplying the target vector with its complex conjugate transpose  $k_p^\dagger$ , [23] [9] which is given as,

$$k_p = \frac{1}{\sqrt{2}} \begin{bmatrix} S_{HH} + S_{VV} \\ S_{HH} - S_{VV} \\ 2S_{HV} \end{bmatrix} \quad (2-8)$$

Therefore,

$$[T] = k_p * k_p^\dagger \quad (2-9)$$

$$[T] = \frac{1}{2} \begin{bmatrix} \langle |S_{HH} + S_{VV}|^2 \rangle & \langle (S_{HH} + S_{VV})(S_{HH} - S_{VV})^* \rangle & \langle (S_{HH} + S_{VV})S_{HV}^* \rangle \\ \langle |(S_{HH} - S_{VV})(S_{HH} + S_{VV})^*| \rangle & \langle |S_{HH} - S_{VV}|^2 \rangle & \langle |(S_{HH} - S_{VV})S_{HV}^*| \rangle \\ \langle |S_{HV}(S_{HH} + S_{VV})^2| \rangle & \langle |S_{HV}(S_{HH} - S_{VV})^*| \rangle & \langle 2|S_{HV}|^2 \rangle \end{bmatrix} \quad (2-10)$$

## 2.2. Orientation angle shifts:

The orientation angle (OA) and the ellipticity describe the polarization state of the electromagnetic wave [9]. Orientation angle is the angle between the ellipse major axis and the horizontal axis and it varies in between 0-180° [9]. For the bio-physical and geo-physical parameters estimation like biomass, stem volume, soil moisture etc. the compensation OA for the PolSAR data is important [24][25]. The OA shifts are more prominent in longer wavelengths. The OA is related to azimuth slope, range slope and radar look angle [26] .

$$\tan \theta = \frac{-\tan \omega}{-\tan \gamma \cos \phi + \sin \phi} \quad (2-11)$$

Where,

$\theta$ -Orientation angle,  $\tan \omega$ - azimuth slope,  $\tan \gamma$ - slope in the ground range,  $\phi$ - radar look angle

The **Error! Reference source not found.** explains the radar geometry of orientation angle with adar look angle  $\phi$ , if the horizontal polarization of the radar system is aligned parallel to horizontal axis (x,y) i.e., in the azimuthal direction and the vertical polarization parallel to vertical plane (v,z); the surface normal N will be in the incidence plane if there is no shift in the orientation angle [24]. Any tilt of the plane in the azimuth direction, the surface normal will no more be in the radar line of sight and causes the shift in the orientation angle along the radar line of sight [24].

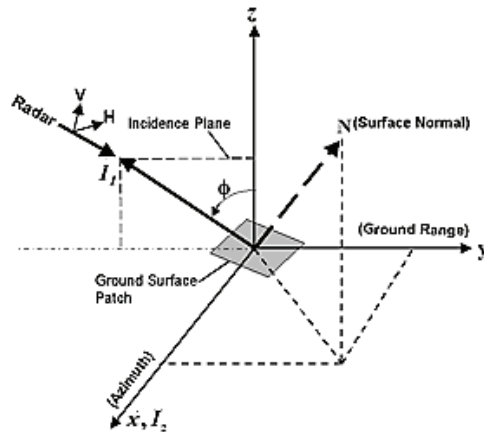


Figure 2-1 : Relation of radar geometry and planes ( source : Lee *et al* [24] )

Schuler *et al.*, in [27] proposed a method for the measurement of topographic profiles using PolSAR data. This method utilizes the orientation angle shifts in the PolSAR data caused by the azimuthal tilts for the generation of topographic profiles using stokes matrix [27]. Lee *et al.*, in [26] proposed two methods of the PolSAR data correction for the backscatter variations induced by the slope in the azimuth direction. In the first method digital elevation model (DEM) is used to measure the orientation angles shifts; the other method, a circular polarization algorithm is used to estimate the orientation angle directly from PolSAR data without the use of DEM [26]. For the compensation of the PolSAR data the estimated orientation angle will be used to rotate the data along the radar line of sight [26]. Circular polarization algorithm, which uses the phase difference between the RR and LL circular polarizations was concluded efficient for the calculation of the orientation angles [26] [24].

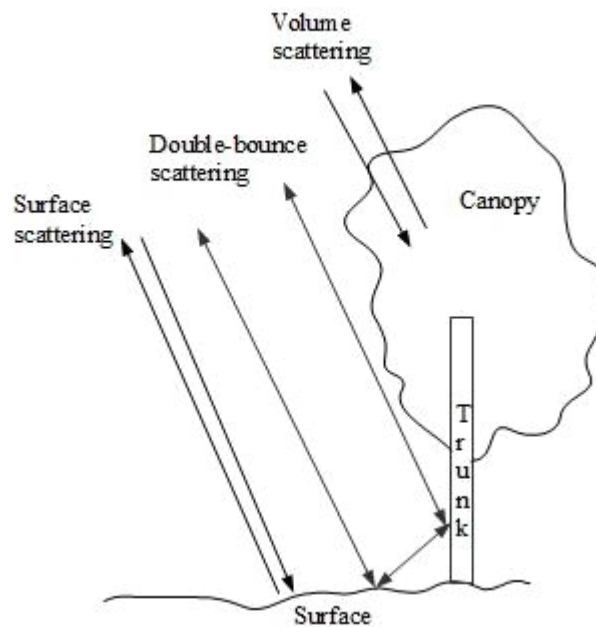


Figure 2-2: Surface, Double-bounce and Volume scattering

Lee *et al.*, in [13] studied the effect of orientation angle shifts on the coherency matrix and covariance matrices. The shift in the orientation angle is zero for reflection symmetrical media, and for non-symmetrical media these shifts result in the increase of cross-polarization power and these shifts make the coherency matrix reflection asymmetric [13]. Therefore they applied the circular polarization algorithm for the estimation of the orientation angles from the PolSAR data and the coherency matrix was rotated along the radar line of sight for the compensation of the shifts. They found that the first element of the coherency matrix  $T_{11}$  is roll-invariant; the  $T_{22}$  element either increases or remains same after the compensation and the  $T_{33}$  element either decreases or remains same after the compensation and the [13]. The increase in the  $T_{22}$  is equal to the decrease in the  $T_{33}$  element as the sum of the diagonal elements i.e., total power is always same [13]. The complex off diagonal element  $T_{23}$  the real part becomes zero and the imaginary

part is roll invariant and no consistent change is found in the remaining off diagonal elements. The rotation of the coherency matrix for orientation angle shifts indeed effects the polarimetric decompositions. It has been found that after the compensation the volume scattering power is reduced and the double-bounce power is increased [13] [28].

### **2.3. Polarimetric decompositions:**

Target decompositions were introduced to distinguish different scattering mechanisms and extract physical information from the targets. Polarimetric decomposition is the technique of separating individual scattering mechanisms that can be identified on the ground which can aid better interpretation[9] [29]. The work of Chandrasekhar on light scattering were the roots for the polarimetric decomposition method developed by Huynen [29] [22] [30].

Different types of polarimetric decomposition methods were proposed based on the scattering matrix and also on the second order statistical representations of scattering matrix. These can be broadly classified in to two types—coherent decompositions and incoherent decompositions [22]. The motive of the coherent decompositions is to express the scattering matrix as a complex sum of individual elementary scattering matrices like sphere, diplane, dipole [29]. The coherent decompositions are well fit for individual scatters or pure targets which scatter completely polarized wave. The coherent target decompositions like Pauli, Ceamaron, Krogager can be applied only for the coherent scatters, which scatter complete polarized wave. Natural objects like vegetation, bare soil, water, crops act like distributed targets and they scatter partially polarized waves [29] [22].

In order to extract various scattering information and accurately relate the scattering to the physical properties of the target, incoherent model based target decompositions were developed for the radar data. Cloude introduced a decomposition method using the covariance matrix and coherency matrix, in which the covariance matrix was decomposed into individual covariance matrices which represent different scattering mechanisms [31] in [23].

Freeman and Durden [11] proposed a decomposition model for PolSAR data without the need for additional ground data by using a three component scattering decomposition model based on reflection symmetry. The first components of this model is volume scattering i.e., scattering through canopy, which is modeled as scattering from cloud of randomly oriented dipoles [11]. The second component is double-bounce scattering which is modeled as dihedral corner reflectors with different dielectric constants, the third component-surface scattering from bare ground is modeled using first order Bragg scattering from a moderately rough surface [11]. This model has been successful in reducing the complexity of other models and the input parameters. This model has the advantage of input parameters is equal to the output parameters under reflection symmetry condition. This model has been successfully implemented to identify the dominant scattering mechanism, discriminating vegetation areas from non-vegetation areas and natural targets from man-made features [11]. Later Freeman developed a new technique by fitting

the PolSAR data to a two component scattering decomposition model [32]. In this technique the volume scattering is modeled as scattering through cloud of randomly oriented cylinder like scatters and the ground scattering component is modeled for the double bounce from a pair of orthogonal surface and surface scattering from Bragg's moderately rough surface with different dielectric constants[32].

Yamaguchi *et al.*, [33] developed a new decomposition model by extending the Freeman three component model based on non-reflection symmetric scattering by adding a new helix scattering component. The helix scattering component was introduced by Krogager and was adapted in the four component decomposition model, which would appear more in complex manmade structures and almost disappears from natural targets [33] [23]. The volume scattering component was modified by considering the relative backscattering powers of the co-pol channels and applying uniform probability density function for cloud of randomly oriented dipoles [33]. The proposed method considered non-reflection symmetry scattering case but still the reflection symmetry was included. The non-reflection symmetry was used to obtain the helix scattering [33] which was found in urban areas with complex structures. For better physical interpretation, a similar approach was applied on the coherency matrix and obtained results were similar to that of the covariance matrix [12]. This method was further extended for better estimation of volume scattering by rotating the coherency matrix and then decomposing in to different scattering components [34]. This method has shown that rotating the coherency for minimization of the cross-pol power and applying the four component decomposition; reduces the volume scattering power and increases the double-bounce scattering power.

## **2.4. Methods of estimating forest biophysical parameters:**

Biomass is defined as the amount of living or dead organic matter present in the vegetation [5] [35]. Biomass is divided in to above ground biomass (AGB) and below ground biomass which can be measured using different techniques like *in-situ* measurements, using remote sensing data [19] [35]. Below ground biomass, for which the remote sensing technique is not helpful needs labor intensive *in-situ* measurements [35].

### **2.4.1. Field measurements:**

- a) Destructive sampling technique is the most accurate and direct method for the estimation of biomass; done by harvesting the vegetation by different component wise like, trees, stems, trunk according to the use [35]. The harvested components are dried and biomass is weighed, which can be done for individual tree or plot wise. This kind of estimation is not recommended for frequent use, as it is time taking and the entire tree has to be removed and the biomass has to be estimated. It is mainly used for developing the biomass equations for individual species type.

- b) Non-destructive sampling is also an *in-situ* technique which doesn't need the harvesting of trees. Parameters like tree height, trunk diameter, basal area are used to estimate biomass using regression equations which relate these parameters and biomass [19][35]. The biomass equations are used to estimate the biomass for individual tree wise or per plot and extrapolated for the forest stand to obtain biomass per unit area. Non-destructive sampling is cost effective when compared to the destructive sampling technique but still a time consuming method. It gets difficult for dense inaccessible forests and also for the tropical forests with varied variety of species this could be a time consuming method [19] which makes remote sensing of the forests inevitable for the monitoring of forest biomass.

#### **2.4.2. Using optical remote sensing data:**

Optical remote sensing technique uses the range of 0.4-2.5 micro meter including the visible spectrum, near and mid infrared portion of EM spectrum, and which measures the reflected solar energy from the Earth surface [36]. Many dimension less measures of vegetation reflectance such as normalized differential vegetation index (NDVI) ratio vegetation index (RVI), Soil adjusted vegetation index (SAVI) were introduced to reduce the effect of soil reflectance and atmospheric attenuation and to predict the quantity and quality of vegetation [37] [36].

Sarker and Nichol [38] used advanced visible and near infrared radiometer sensor (AVNIR-2) of ALOS for the estimation of biomass. For this purpose the individual bands spectral reflectance, simple band ratios, the texture measurements and ratio of texture measurements were related to the field estimated biomass using regression analysis. A similar kind of approach was used by Nichol and Sarker [39] where a combination of multi sensor high resolution optical data of Advanced visible and near infrared radiometer (AVNIR-2) of ALOS and High resolution Geometric (HRG) of SPOT-5 were used for estimating biomass over sub-tropical forest. For this purpose spectral reflectance from each individual band of each sensor, simple band ratios and texture estimation of each band for individual sensors and for combination was used to relate with the field estimated biomass [39]. Both the studies concluded that the ratio of texture measurements were reliable for estimation of biomass from optical data. Ullah *et al.* [37] used medium resolution imaging spectrometer (MERIS) for the estimation of biomass and nitrogen quantities for grasslands by comparing various vegetation indices.

Optical remote sensing techniques for the estimation biophysical parameters have been studied and summarized by Wulder [40]. The ineffectiveness of the optical remote sensing techniques to relate directly the optical data to the biophysical parameters are making way for the use of other, more reliable techniques like radar remote sensing (SAR) and Lidar [36][41].

#### **2.4.3. Using Lidar data:**

Laser altimetry or Light detection and ranging (Lidar) is an active remote sensing sensor which measures the time difference of sent and received signal to measure the distance of the target

from the sensor [42]. Many studies have been demonstrated the usefulness and accuracy of Lidar data for topographic measurement and also for the estimation of forest parameters like tree height [42].

Drake *et al.* in [43] applied large footprint LVIS (Laser vegetation imaging system) sensor for the estimation of AGB and structural parameters of tropical forests. In this study the individual footprint level and plot level analysis was made to estimate the tree height. This tree height was used in the allometric equations for the estimation of AGB at footprint level and at plot level [43].

J.Boudreau *et al.* [44] compared the AGB estimates from Lidar data obtained from PALS (Portable airborne laser system) sensor and GLAS (Geoscience laser altimeter system) sensor of ICESat. The height information obtained from both sensors was fitted to the allometric equations for the estimation of AGB and compared with field estimates. This study was successful in showing that the space borne laser systems are capable of estimating forest biophysical parameters at a regional scale. Kronseder *et al.* in [45] used small footprint airborne Lidar for the estimation of AGB in forests in Central Kalimantan at different degradation levels. For this study they analyzed the 3-D point cloud generated from the Lidar data and related it to field estimated AGB plot wise and concluded that this kind of approach is useful for the AGB estimations for different forest types and at different degradation levels [45]. These studies based on larger footprint Lidar and small footprint Lidar applied for different forest types show that the potential of Lidar remote sensing for the more accurate for the monitoring and estimating the biophysical parameters of vegetation.

#### **2.4.4. Using radar data:**

Many studies have been carried out to relate the forest parameters like AGB, stem volume, height using SAR data which showing the capability of SAR data for the use of vegetation monitoring. Le Toan *et al.* in [46] related the radar backscattering of NASA/JPL SAR to the forest biomass at multiple frequencies. The P, L, C band data with HH, HV and VV and HH, VV polarizations of DLR SAR X-band were related to biomass estimated from the field using regression analysis. The experimental results show that the L-band and P-band have good correlation with the field estimated biomass when compared to the C-band and X-band. Lo Seen *et al.* in [47] used multi-frequency SAR data to retrieve the tropical forest parameters P, L and C-band data of AIRSAR. For this purpose they used band ratio of different wavelengths and different polarizations to reduce the topographic effects and compared to the basal area of the forest stand.

Paloscia *et al.* in [48] discussed the potential of space borne radar satellites to predict the biomass of vegetation using the C-band of ERS-1 and L-band of JERS-1 data. The data was collected was collected VV and HH polarizations for ERS and JERS satellite respectively and air bone SAR data was collected in dual polarizations in C, L and P-bands and related to the field biomass data using regression analysis. The experimental results concluded that the L-band and P-band and in good agreement with the field data and C-band data can used to differentiate different crops [48].

Morel *et al.* in [49] used L-band dual polarization ALOS-PALSAR data for the estimation AGB in forest and palm plantations in Sabah area of Malaysia. One of the important objectives of this study is to differentiate palm plantations from the forest area using HH, HV and a ratio of HV/HH is considered to reduce the topographic effects and the classification is done the data using the imagery which showed satisfactory result. The experiment result showed that the HV polarization is correlated with field estimated biomass and this was used in the regression analysis to estimate the biomass, which shows the potential of L-band for monitoring of forests.

Mitchard *et al.* in [50] used ALOS-PALSAR fine beam dual polarization (HH,HV) data to estimate the AGB of the tropical savanna forests. The study sites were selected at four different locations in Africa with different forest structures. The results are the L-band HV polarization is more sensitive to biomass than the HH polarization and the relation is consistent in all the four site irrespective of different forest structure and also reported better saturation limits [50].

Xu *et al.* [20] applied three component decomposition [11] on the quad-pol data of RADARSAT-2 data for extracting volume scattering, double-bounce and surface scattering information and related these components to the field estimated data for the extraction biomass related parameters. A similar kind of approach has been adapted in Tan *et al.* [21] compared field estimated biomass with the ALOS-PALSAR quad-pol data, TerraSAR-X and Lidar data. Four component decomposition of Yamaguchi *et al.* [12] was used to identify volume scattering, surface scattering and double-bounce scattering from both PALSAR and TerraSAR-X data [21]. Allometric equations were used to estimate biomass from the Lidar data [21]. Ratio of volume scattering to surface scattering was related with field estimated biomass for both L-band and X-band data using regression analysis. This study concluded that these biomass estimates are comparable with that of Lidar data [21].

Hsu *et al.* in [51] applied radiative transfer theory (RT) to interpret the backscattering from pine forest. RT theory consists of RT equations which are used to observe the EM wave propagation through multiple layer scattering media and to calculate the backscattering from each layer. Liang *et al.* developed a model for backscattering from multilayer and multi species vegetation using RT theory. The idea behind this model development is to improve the previously existing model MIMCS [15] for vegetation with different species and also to include the overlapping canopies. Burgin *et al.* [52] proposed a backscattering model of multilayer and multispecies vegetation using wave theory, which use distorted Born approximations and Maxwell equations for scattered medium.

Attema *et al.* [14] developed a semi-empirical model called Water Cloud Model (WCM) for modeling the radar backscatter from vegetation. Model assumes vegetation canopy as water cloud containing water droplets modeled as vegetation matter, over a moderately rough surface with dielectric constant [14]. This model considered backscattering from surface and the canopy only and ignored the higher order scattering interactions and scattering through canopy gaps [53][16]. WCM is simpler and does not need many input parameters when compared to other models

developed later. WCM has been adapted for the estimation biophysical parameters of boreal forests, tropical forests [18] [4].

Santoro *et al.* [53] used a model similar to WCM called Interferometric WCM which includes canopy gaps using coherence generated from ERS-1 and ERS-2 repeat pass multi-temporal interferometric SAR data for the estimation the stem volume. Later Santoro *et al.* [18] assessed the stem volume retrieval of Boreal forests from JERS-1 L-band HH polarization SAR data. For this purpose the inverted WCM which included canopy gaps was used to estimate stem volume from radar backscatter [18]. The seasonal effects on backscatter of L-band of JERS-1 in boreal forest and effects on the retrieval stem volume were assessed by Santoro *et al.* [17]. HH polarization L-band multi temporal datasets were used to retrieve stem volume using WCM and to assess the seasonal effects on the retrieved stem volume [17]. This study also suggested that retrieval of stem volume during the winter or frozen or rainfall conditions would produce erroneous results. Santoro *et al.* [4] used hyper-temporal series of ENVISAT-ASAR ScanSAR images for the retrieval of growing stock volume. A straight forward BIOMSAR algorithm which consists of two stages, generation of stack calibrated and geocoded backscatter images from hyper temporal ASAR C-band data [4]. The second stage is to inverse the backscattering values using WCM which includes canopy gaps. Both the above studies suggested that WCM is reliable for inversion of biophysical parameters. Kumar *et al.* [16] estimated the AGB from Envisat-ASAR dual polarisation data for tropical forest. The main aim of this study is to estimate AGB from forest backscatter form individual ASAR images and also using coherence generated from the interferometric SAR. Reasonable estimates were found from interferometric data and also from ASAR backscatter [16].



### **3. STUDY AREA:**

The study area of this research is focussed on Dudhwa National park area in Uttar Pradesh state of Northern India. The area covered by the park is 68032 ha and lies between 28°18'-28°42' N latitudes and 80°28'-80°57' E longitudes [19][54] [55]. The vegetation here is of moist sub-tropical broad leaf forests, and is finest Sal forest in India and it is a home for diversified flora and fauna. [54] [55]. The present study area Dudhwa national park is shown in the Figure (3-1).

#### **3.1. Significance of the study area:**

The Dudhwa national park forms the part of Dudhwa tiger reserve along with the Kishanpur wild life sanctuary and Katemaighat wildlife sanctuary [54]. Mohana and suheli rivers flow through the Dudhwa national park [54]. Dudhwa national park is home for diversified flora and fauna. It is a home for five different species of deer's found in the country and most of the tiger population in Uttar Pradesh state is found here [54]. The vegetation found in the Dudhwa national park is of moist sub-tropical forest consisting mainly Sal forest and home for finest Sal forests in the country. Along with Sal forest different plantations like Eucalyptus, Teak, Shisham are found in the study area. Important forest types found in Dudhwa national park are Northern Tropical Semi Evergreen forest, Northern Indian Moist Deciduous forest, Tropical Seasonal Swamp forest and Northern Tropical Dry Deciduous forest [55] [19]. The area is dominated with Sal forest along with other important species like Jamun, Shisham, Asna are also found [54] [19]. Increased settlements in the forested area and converting the forested areas in to agriculture land is increasing which effects the vegetation of the in the area [19]. This study area is selected due to its varied vegetation types. When using a longer wavelength band like L-band, different kinds of scattering mechanisms can be observed and is suitable for the monitoring of the vegetation parameters. The dense canopy contributes to the volume scattering while the longer trunks and the underlying ground provides the double bounce scattering and surface scattering which makes the Dudhwa national park a better choice for the modelling of biophysical characteristics of the vegetation using the PolSAR data.

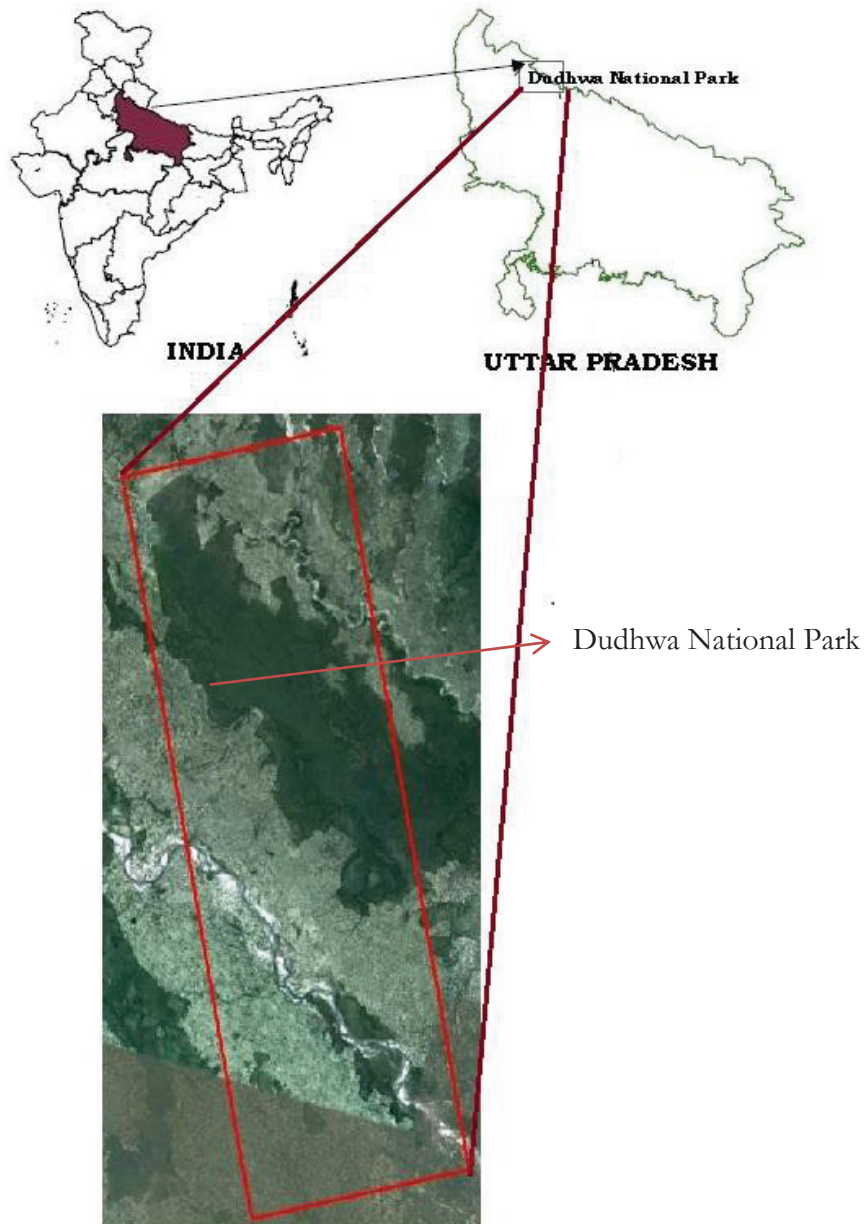


Figure 3-1 : Figure 1 : PolSAR data foot print shown on the Google Earth image with location in India ( Source : India and Uttar Pradesh images from S Kumar [19] and Google Earth image of 22<sup>nd</sup> Feb 2012)

Figure 3-1 shows the ALOS-PALSAR foot print (red colour box) for the data collected over Dudhwa national park and the Google Earth image of the study area.

## 4. MATERIALS AND METHODS

This chapter is divided into four sections; the first section gives the descriptions of the dataset used in the study i.e., ALOS-PALSAR. The second section gives the plot details for the *in-situ* field data. The third section is overview of the methodology applied in this study. The last section is detailed description of the methodology.

### 4.1. Dataset description:

ALOS-PALSAR data in L-band is used in this study. Advanced Land Observation Satellite (ALOS) is a Japans largest satellite developed by Japan aerospace exploration agency (JAXA), carrying three instruments – Panchromatic Remote sensing Instrument for Stereo Mapping (PRISM), Advanced Visible and Near-Infrared Radiometer type II [56]. The third instrument which is used in present study is Phased Array L-band Synthetic Aperture Radar (PALSAR) which was developed by JAXA and Japan Resources Observation Systems Organisation (JAROS) and was in operation from 2006 - 2011. The PALSAR instrument operates in (i) fine beam mode with single or dual or quad polarizations (ii) scanSAR mode with single polarizations (HH or VV). The Table 4-1 gives the characteristics of the data.

Table 4-1: Data characteristics

Satellite-Sensor	ALOS – PALSAR
Date of acquisition	31 October 2009
Polarisation	Quad-polarization (HH+HV+VH+VV)
Node	Ascending
Wavelength	23.5 cm
Incidence angle	25.6
Orbit	20081
Frame	560
Product level	1.1
Range and Azimuth spacing in SLC format	9.265(Range)×3.779(Azimuth)
Centre latitude	28.40295
Centre longitude	80.66890

PALSAR data of level 1.1 was used in this study. Level 1.1 indicates that the data is not geocoded and in single look complex format (SLC) and each pixel in this format is a complex numbers. The L-band data due to its longer wavelength penetrates more through the vegetation canopy and provides the information of the ground and trunk and is more suitable for the remote sensing of forests.

## 4.2. Forest inventory data collection:

Forest inventory data was collected for Dudhwa National Park area from 39 site clusters and each cluster consisting of 4 plots and a total of 152 plots. Each plot was collected for an area 0.1 ha. The details of the forest inventory data collected in March 2008, stratum wise clusters and plots are given in the Table 4-2. Figure 4-1 shows the false colour composite of Landsat-7 ETM+ sensor image with *in-situ* data collected in the Dudhwa National Park study area. (The *in-situ* measurements data were provided by the Forestry and Ecology division, IIRS)

Table 4-2 : stratum wise number of clusters and plots

Forest Type	No of Clusters	No of plots
Asidha Plantations	1	3
Eucalyptus	3	11
Mixed Forest	5	20
Sal Forest	20	78
Teak Plantations	5	20
Shisham	4	16
Jamun	1	4

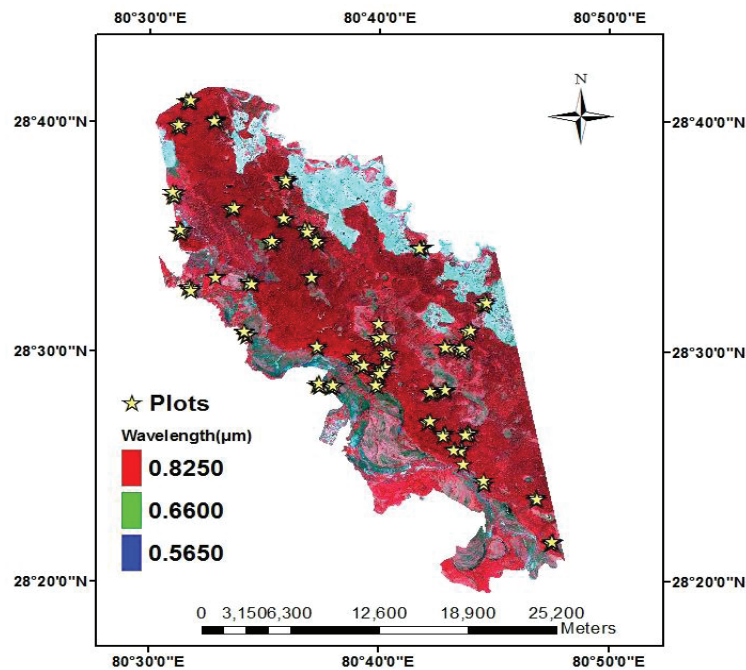


Figure 4-1 : ETM+ FCC imaging showing the *in-situ* data collected in the Dudhwa National Park

### 4.3. Methodology Flow Chart:

The Figure 4-2 shows the methodology used in the present study.

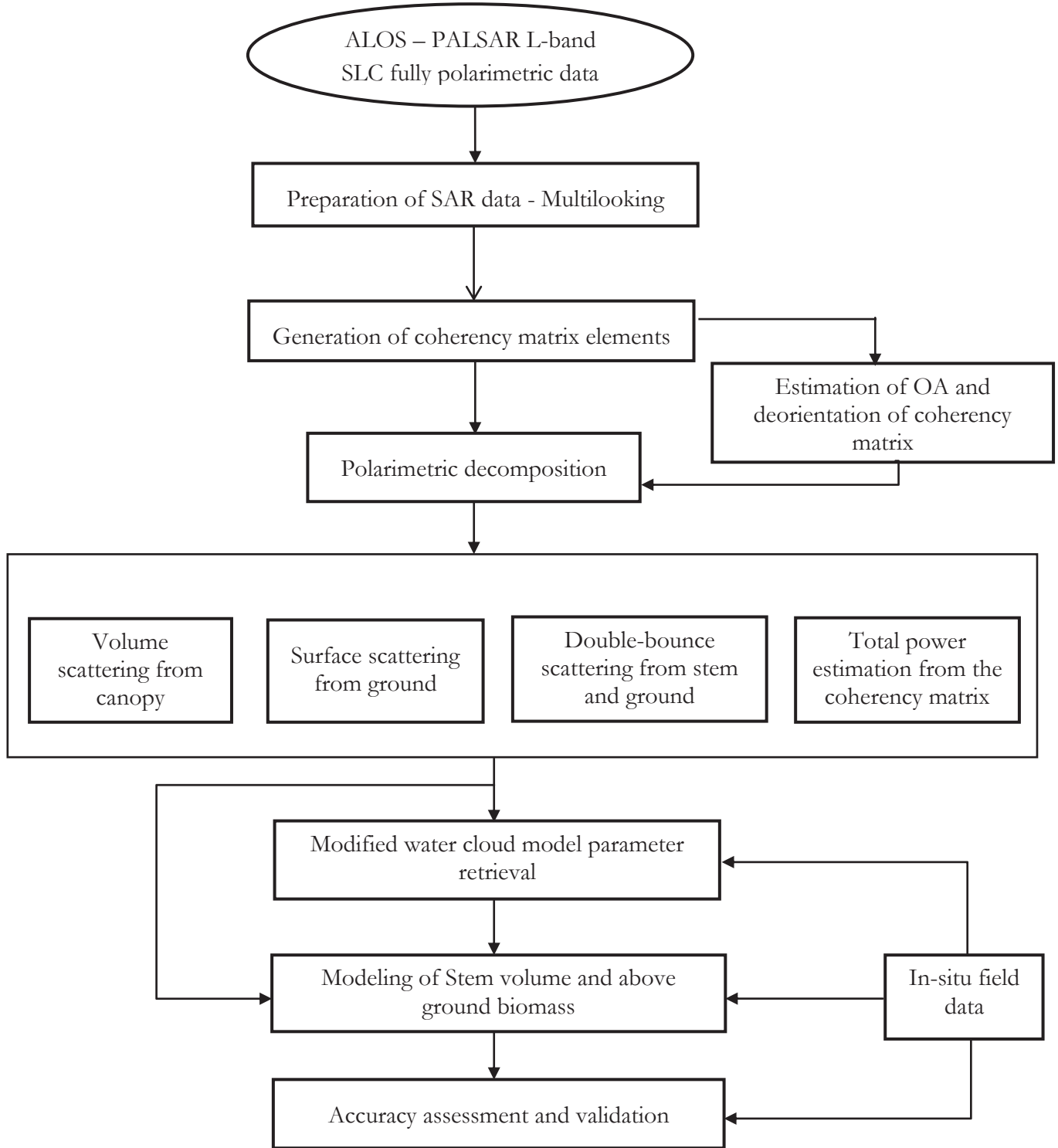


Figure 4-2 : Methodology Flow-chart

## 4.4. Methodology:

### 4.4.1. Data pre-processing:

The ALOS-PALSAR data used in this study is of level 1.1 which is single look complex (SLC) data acquired in quad-polarization (HH, HV, VH, VV) in L-band data with wavelength 23.5 cm data. The level 1.1 indicates that the data is not geocoded and in scattering matrix format. The azimuth and range resolutions are 3 m and 21 m respectively in slant range and compressed format and also contains speckle. In order to convert the data from slant range to ground range, multilooking of the SLC data has been done with 6 looks in the azimuth and 1 look in the range direction to achieve a round range resolution of approximately 22 m. Figure (4-3) shows the SAR image in SLC format and the image after multilooking.

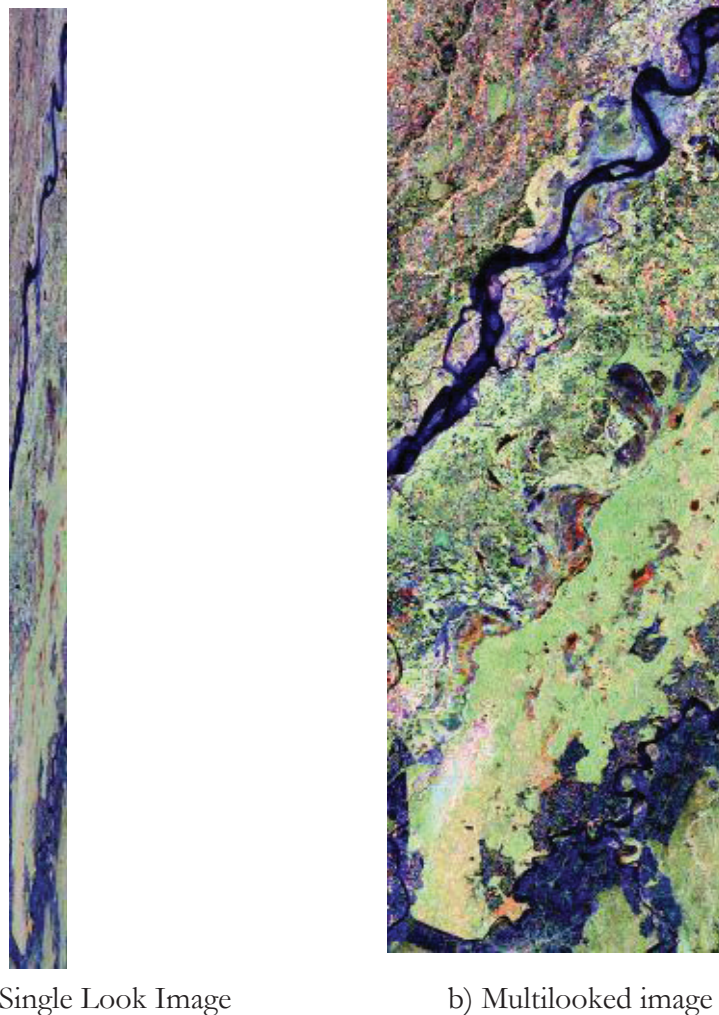


Figure 4-3 Pauli colour coded SAR images in SLC format and Multilooked image with HH-VV, HV, HH+VV in Red, Green and Blue bands respectively

#### 4.4.2. Coherency matrix generation from the scattering matrix:

The coherency matrix  $T$  is generated from the vectorized form of the scattering matrix  $[S]$  using Pauli's target vector  $k_p$ . The coherency matrix is generated by multiplying the target vector with its complex conjugate transpose  $k_p^\dagger$  [57].

$$k_p = \frac{1}{\sqrt{2}} \begin{bmatrix} S_{HH} + S_{VV} \\ S_{HH} - S_{VV} \\ 2S_{HV} \end{bmatrix}$$

Therefore,

$$T = k_p * k_p^\dagger$$

$$[T] = \frac{1}{2} \begin{bmatrix} \langle |S_{HH} + S_{VV}|^2 \rangle & \langle (S_{HH} + S_{VV})(S_{HH} - S_{VV})^* \rangle & 2\langle (S_{HH} + S_{VV})S_{HV}^* \rangle \\ \langle (S_{HH} - S_{VV})(S_{HH} + S_{VV})^* \rangle & \langle |S_{HH} - S_{VV}|^2 \rangle & 2\langle (S_{HH} - S_{VV})S_{HV}^* \rangle \\ 2\langle |S_{HV}(S_{HH} + S_{VV})|^2 \rangle & 2\langle |S_{HV}(S_{HH} - S_{VV})|^2 \rangle & 4\langle |S_{HV}|^2 \rangle \end{bmatrix} \quad (4-1)$$

Here,  $\langle \rangle$  represents the average over the complete data,  $\dagger$  represents the complex conjugate transpose;  $*$  represents the complex conjugate. The sum of the diagonal elements is called span or the total power.

#### 4.4.3. Decomposition of Coherency matrix:

The coherency matrix obtained is decomposed into various scattering mechanisms like volume scattering, surface scattering and double-bounce scattering using the decomposition algorithm developed by Yamaguchi *et al.* [12]. This algorithm fits the polarimetric data in to four components – volume scattering, surface scattering or odd-bounce scattering, double-bounce scattering and helix scattering which doesn't consider reflection symmetry condition. The double-bounce scattering which appears due to ground stem interactions from the vegetation was used in this study for extending the WCM for higher order interactions along with volume and surface scattering.

The mathematical modelling of this decomposition algorithm uses the basic coherency matrices of volume scattering, surface scattering, double-bounce scattering and helix scattering components. The total power or the span is equal to the weighted sum of all these individual powers.

$$\langle [T] \rangle = f_s \langle [T] \rangle_{surface} + f_d \langle [T] \rangle_{double} + f_v \langle [T] \rangle_{volume} + f_c \langle [T] \rangle_{helix} \quad (4-2)$$

Here,

$\langle [T] \rangle$  is the coherency matrix.  $\langle [T] \rangle_{\text{surface}}$ ,  $\langle [T] \rangle_{\text{double}}$ ,  $\langle [T] \rangle_{\text{volume}}$  and  $\langle [T] \rangle_{\text{helix}}$  are the basic coherency matrices for surface scattering, double-bounce, volume and helix scattering respectively;  $f_s$ ,  $f_d$ ,  $f_v$  and  $f_c$  are the respective expansion coefficients [12]. The basic coherency matrices are used in the Equation (4-2) to obtain the respective expansion factors for surface scattering, double-bounce, volume scattering and helix scattering.

a. Volume scattering:

The volume scattering is modelled by employing a randomly oriented dipoles model with probability density function for better modelling of scattering from tree trunks and branches [12] [33]. The basic coherency matrix for volume scattering given as in Yamaguchi *et al.* [12].

$$\langle [T] \rangle_{\text{volume}} = \frac{1}{4} \begin{bmatrix} 2 & 0 & 0 \\ 0 & 1 & 0 \\ 0 & 0 & 1 \end{bmatrix} \quad (4-3)$$

b. Surface scattering:

Bragg's surface model is employed to model the scattering from a moderately rough surface, the basic coherency matrix for surface scattering was proposed as in Yamaguchi *et al.* [12].

$$\langle [T] \rangle_{\text{surface}} = \begin{bmatrix} 1 & \beta^* & 0 \\ \beta & |\beta|^2 & 0 \\ 0 & 0 & 0 \end{bmatrix} \quad \text{With } \beta = \frac{R_h - R_v}{R_h + R_v} \quad (4-4)$$

Here  $R_h$ ,  $R_v$  are the Fresnel reflection coefficients for horizontal and vertical polarizations respectively.

c. Double-bounce scattering:

The double-bounce scattering which occurs due to interaction like ground-trunk is modelled as backscattering from dihedral corner reflector whose basic coherency matrix is given as [12].

$$\langle [T] \rangle_{\text{double}} = \begin{bmatrix} |\alpha|^2 & \alpha & 0 \\ \alpha^* & 1 & 0 \\ 0 & 0 & 0 \end{bmatrix} \quad \text{With } \alpha = \frac{S_{HH} + S_{VV}}{S_{HH} - S_{VV}} \text{ and } |\alpha| < 1 \quad (4-5)$$

d. Helix scattering:

The helix scattering component which is additionally added in the four component decomposition and was ignored in the three component decomposition [11] under reflection symmetry i.e.,  $\langle S_{HH} S_{HV}^* \rangle = \langle S_{VV} S_{HV}^* \rangle = 0$  [33][12].

The basic coherency matrix for the helix scattering which was adapted from the Krogager decomposition is given as [12].

$$\langle [T] \rangle_{\text{helix}} = \frac{1}{2} \begin{bmatrix} 0 & 0 & 0 \\ 0 & 1 & \pm j \\ 0 & \pm j & 1 \end{bmatrix} \quad (4-6)$$

Four component decomposition algorithm:

By substituting the respective basic coherency matrices in Equation (4-2) is the four component decomposition algorithm.

$$\langle [T] \rangle = f_s \begin{bmatrix} 1 & \beta^* & 0 \\ \beta & |\beta|^2 & 0 \\ 0 & 0 & 0 \end{bmatrix} + f_d \begin{bmatrix} |\alpha|^2 & \alpha & 0 \\ \alpha^* & 1 & 0 \\ 0 & 0 & 0 \end{bmatrix} + \frac{f_v}{4} \begin{bmatrix} 2 & 0 & 0 \\ 0 & 1 & 0 \\ 0 & 0 & 1 \end{bmatrix} + \frac{f_c}{2} \begin{bmatrix} 0 & 0 & 0 \\ 0 & 1 & \pm j \\ 0 & \pm j & 1 \end{bmatrix} \quad (4-7)$$

The respective expansion coefficients for volume, double-bounce, helix and surface scattering  $f_v, f_d, f_c, f_s$  are given as [12]

$$f_v = 8\langle |S_{HV}|^2 \rangle - 4|\text{Im}\langle (S_{HH} - S_{VV})S_{HV}^* \rangle| \quad (4-8)$$

$$f_d = \frac{1}{2}\langle |S_{HH} - S_{VV}|^2 \rangle - 2\langle |S_{HV}|^2 \rangle \quad (4-9)$$

$$f_c = 2|\text{Im}\langle (S_{HH} - S_{VV})S_{HV}^* \rangle| \quad (4-10)$$

$$f_s = B - \frac{|C|^2}{A} \quad (4-11)$$

Where,

$$A = \frac{1}{2}\langle |S_{HH} - S_{VV}|^2 \rangle - 2\langle |S_{HV}|^2 \rangle,$$

$$B = \frac{1}{2}\langle |S_{HH} + S_{VV}|^2 \rangle - 4\langle |S_{HV}|^2 \rangle, C = \frac{1}{2}\langle (S_{HH} + S_{VV})(S_{HH} - S_{VV})^* \rangle$$

The corresponding scattering powers are obtained by

$$P_s = f_s(1 + |\beta|^2) \quad (4-12)$$

$$P_d = f_d(1 + |\alpha|^2) \quad (4-13)$$

$$P_v = f_v \quad (4-14)$$

$$P_c = f_c \quad (4-15)$$

$$\text{The total scattering power} \quad P_t = P_c + P_d + P_v + P_s \quad (4-16)$$

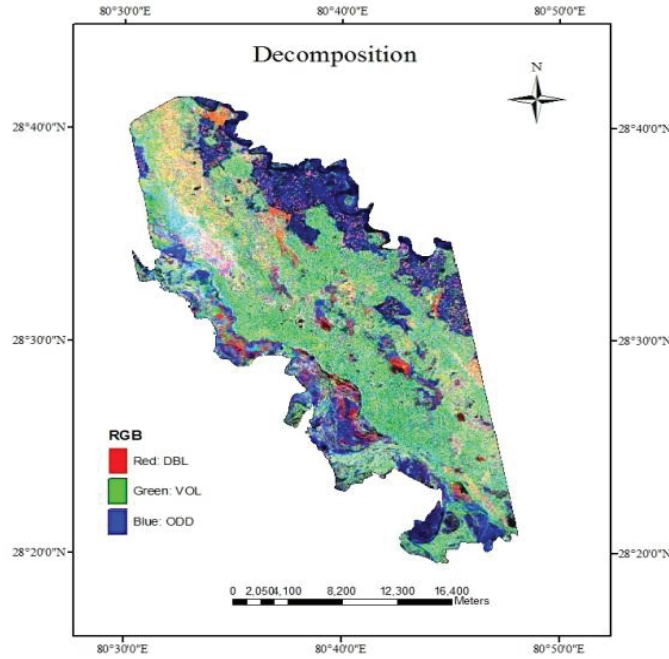


Figure 4-4 : Decomposition components shown in RGB. Red – double bounce (DBL), Green - Volume scattering (VOL), Blue - Odd bounce or Surface scattering (ODD)

Figure (4-4) shows the decomposition components displayed in RGB with Red-double bounce (DBL), Green – Volume scattering (VOL) and Blue – Surface or odd-bounce scattering (ODD).

#### 4.4.4. Calculation of OA shift using coherency matrix:

In the next step the coherency matrix generated from the Equation (4-1) is used to estimate the orientation angle (OA) shifts. The coherency matrix is deoriented by rotating the coherency matrix for compensating the shifts in the OA. The OA shifts can be compensated by rotating the coherency matrix about the line of sight by negative of the estimated OA, using a unitary matrix and OA is affected by both terrain slopes and azimuth slopes. Lee *et al.* [26] proposed a method based on the circular polarization technique for the estimation of the OA from the PolSAR data which is

$$\eta = \frac{1}{4} \left[ \tan^{-1} \left( \frac{-4 \operatorname{Re}((S_{HH} - S_{VV})S_{HV}^*)}{-(|S_{HH} - S_{VV}|^2 + 4|S_{HV}|^2)} \right) + \pi \right] \quad (4-17)$$

Where,  $\theta = \begin{cases} \eta, & \text{if } \eta \leq \pi/4 \\ \eta - \pi/4, & \text{if } \eta > \pi/4 \end{cases}$  here,  $\operatorname{Re}(\cdot)$  represents the real part and  $\theta$  represents the angle shift in the orientation and the estimated orientation angle ranges from  $-\pi/4$  to  $\pi/4$ [28] [13].

The OA rotation on coherency matrix in is obtained by unitary matrix transformations

$$[\tilde{T}] = [U][T][U^T] \tag{4-18}$$

With,  $[U] = \begin{bmatrix} 1 & 0 & 0 \\ 0 & \cos 2\theta & \sin 2\theta \\ 0 & -\sin 2\theta & \cos 2\theta \end{bmatrix}$  Where  $[U]$  is the unitary rotation operator and  $[\tilde{T}]$  is the coherency matrix after rotation.

**4.4.5. Decomposition of the coherency matrix after deorientation:**

The decomposition algorithm of Yamaguchi *et al.* [12] from the Equation (4-16) is applied on the coherency matrix which is compensated for the OA shifts to obtained decomposition components – volume scattering, double-bounce scattering, surface scattering with the no effect of OA shifts.

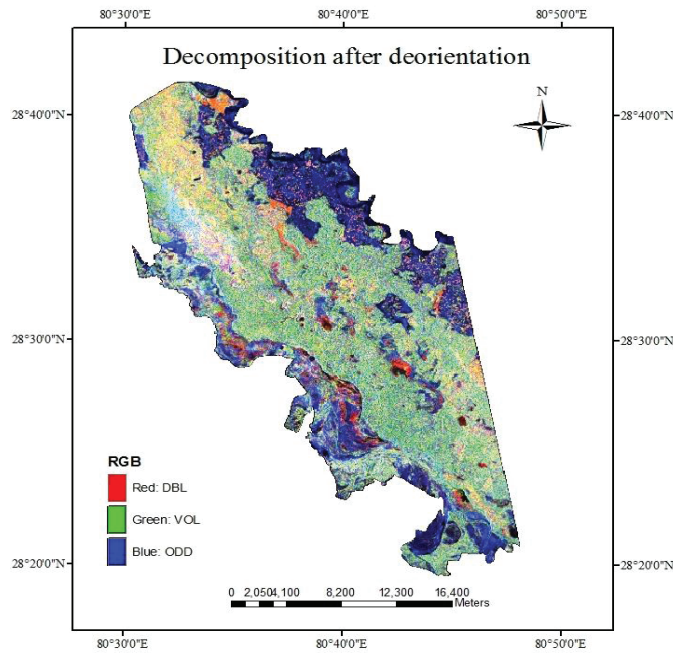


Figure 4-5 : Decomposition components obtained after deorientation displayed in RGB. Red- Double-bounce (DBL), Green-Volume scattering (VOL), Blue-surface scattering (ODD)

Figure (4-5) is the RGB image of the decomposition components obtained by using the OA shifts compensated coherency matrix with Red, Blue, Green as Double-bounce (DBL), Volume (VOL) and Surfaces (ODD) scattering respectively. A Boxcar filter [23] of 15×15 window size applied to reduce the effect of speckle noise. The obtained results which are filtered using the Boxcar filter are used in the further analysis.



## 5. MODELLING APPROACH: WATER CLOUD MODEL AND EXTENDED WATER CLOUD MODEL

This chapter is divided into three sections. The modelling approach using WCM and WCM with canopy gaps is discussed in the first section. The extended WCM for the higher order scattering mechanisms like ground stem interactions is discussed in the second section. The second section gives the detailed description of the use of the PolSAR data in the water cloud modelling approach for forest biophysical parameters estimation.

### 5.1. Water Cloud Model (WCM):

The Water Cloud Model developed by Attemma and Ulaby [14] describes the relationship between the forest parameters and forest backscatter. The model assumes that vegetation behaves like a homogenous medium like a water cloud filled with water droplets over a horizontal plane which is modeled as ground and the scattering elements contained in water cloud as water droplets [14][19][16]. The incoming incident energy is partly reflected back to the sensor and partly transmitted to the lower vegetation layer with attenuation and the water cloud model in the terms of total forest backscatter, backscatter from vegetation and from ground are related as [16].

$$\sigma_{for}^{\circ} = \sigma_{veg}^{\circ} + \sigma_{gr}^{\circ} T_{tree} \quad (5-1)$$

$\sigma_{for}^{\circ}$  - Forest backscatter

$\sigma_{veg}^{\circ}$  - Backscatter of vegetation

$\sigma_{gr}^{\circ}$  - Backscatter from ground

$T_{tree}$  - Two way tree transmissivity

The water cloud model assumes vegetation layer as homogenous medium and the vegetation matter contained in the cloud are identical [19]. Higher order scattering mechanisms such as double-bounce which occurs due to the interaction of micro wave with the stem and ground are not considered [19]. The scattering through the canopy gaps are also not considered [17][18].

A similar model based on the radiative transfer theory for including the gaps in the canopy was developed. The equation for the water cloud model including canopy gaps as in [16][18][4].

$$\sigma_{for}^{\circ} = (1 - \eta)\sigma_{gr}^{\circ} + \eta[\sigma_{gr}^{\circ} T_{tree} + \sigma_{veg}^{\circ} (1 - T_{tree})] \quad (5-2)$$

Where,  $\eta$  is the area fill factor.

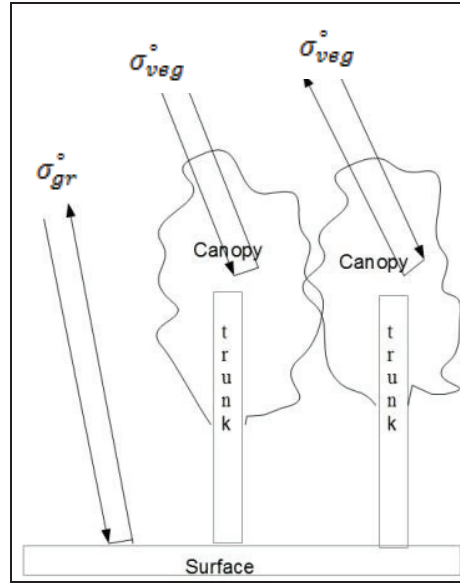


Figure 5-1 : Water Cloud Model showing backscattering from canopy  $\sigma_{veg}^\circ$  and backscattering from ground  $\sigma_{gr}^\circ$

The Figure (5-1) shows the water cloud model which considers only two scattering mechanisms. The incident wave reaches the canopy and interacts with the canopy and reflects back to the sensor and it is represented as  $\sigma_{veg}^\circ$ . The incident wave interacts with the ground and reflects back to the canopy which is represented as backscattering from ground i.e.,  $\sigma_{gr}^\circ$ .

a. Properties of the water cloud model including canopy gaps:

$\sigma_{gr}^\circ (1 - \eta)$  represents the scattering from the ground through the canopy gaps, with  $\eta$  representing the fraction of ground covered by the canopy and  $(1 - \eta)$  representing the fraction of the ground not covered by the canopy,  $\eta \sigma_{gr}^\circ T_{tree}$  represents the backscattering from the ground and attenuated by the canopy, and  $\eta \sigma_{veg}^\circ (1 - T_{tree})$  represents the backscattering through vegetation layer[16].

The two way tree transmissivity  $T_{tree}$  which explains amount of total power transmitted to the lower layer can be expressed as the inverse of exponential of product of two way attenuation per meter “ $a$ ” and the thickness of the attenuating layer “ $b$ ” as  $e^{-\alpha h}$ , and the Equation (5-2) can be rearranged in the terms of  $a$  and  $b$  as [19][17].

$$\sigma_{for}^\circ = (1 - \eta)\sigma_{gr}^\circ + \eta[\sigma_{gr}^\circ e^{-\alpha h} + \sigma_{veg}^\circ (1 - e^{-\alpha h})] \quad (5-3)$$

Equation (5-3) can be rearranged to highlight the backscattering from vegetation and ground

$$\sigma_{for}^\circ = \sigma_{gr}^\circ ((1 - \eta) + \eta e^{-\alpha h}) + \eta \sigma_{veg}^\circ (1 - e^{-\alpha h}) \quad (5-4)$$

If the two way forest transmissivity is represented as  $T_{for}$ , it can be expressed in the terms of area fill factor as

$$T_{for} = [1 - \eta + \eta e^{-\alpha h}] \quad (5-5)$$

So, the Equation (5-4) can be rearranged in the terms of forest transmissivity as

$$\sigma_{for}^{\circ} = \sigma_{gr}^{\circ} T_{for} + \sigma_{veg}^{\circ} (1 - T_{for}) \quad (5-6)$$

The two-way forest transmissivity  $T_{for}$  can be expressed in the terms of stem volume “ $v$ ” and empirically defined coefficient “ $\beta$ ” as [17][18].

$$T_{for} = e^{-v\beta} \quad (5-7)$$

The two way attenuation of the forest can be expressed as the exponential of product of stem volume “ $v$ ” and empirically defined coefficient “ $\beta$ ” as in [4][18] [19] [17]

$$\sigma_{for}^{\circ} = \sigma_{gr}^{\circ} e^{-\beta v} + \sigma_{veg}^{\circ} (1 - e^{-\beta v}) \quad (5-8)$$

## 5.2. Extended Water cloud model (WCM) for higher order interactions:

The above mentioned WCM approaches doesn't consider the higher order interaction such as double-bounce which mainly occurs due to the ground stem interaction and these should be accounted when considering a wavelength of region L-band [8]. The present WCM including canopy gaps was further extended in the following approach

### 5.2.1. Backscattering from the ground-stem interaction from the canopy gaps:

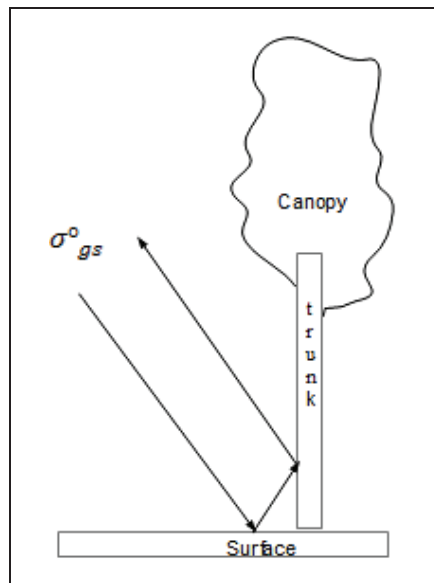


Figure 5-2 : Ground-Stem interaction  $\sigma_{gs}^{\circ}$  from canopy gaps

The Figure (5-2) explains the incoming wave hitting the ground and reflected toward the trunk and returns back to the sensor through the canopy gaps.

The backscattering contributions from the ground-stem interactions from the canopy gaps are considered as

$$(1 - \eta)\sigma_{gs}^{\circ} \quad (5-9)$$

Here,

$(1 - \eta)$  Represents the fraction of the ground not covered by the canopy and  $\sigma_{gs}^{\circ}$  is the backscattering from ground-Stem interaction.

### 5.2.2. Backscattering from the stem ground interaction through the canopy:

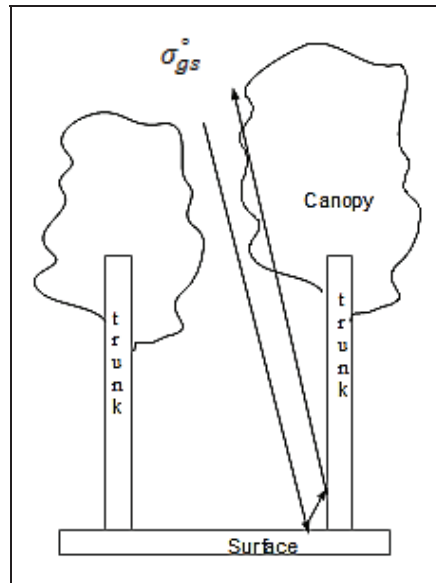


Figure 5-3 : Ground-Stem interaction  $\sigma_{gs}^{\circ}$  through canopy

As shown in the Figure (5-3) the incoming wave interacts with the ground and reflected towards the stem and reflects back to the antenna.

This contribution of ground-stem interactions are considered as

$$\eta\sigma_{gs}^{\circ} T_{tree} \quad (5-10)$$

Here,  $\eta$  represents the fraction of ground covered by the canopy,  $\sigma_{gs}^{\circ}$  is the backscattered wave due to ground-stem interactions and  $T_{tree}$  is the two-way tree-transmissivity.

So, the extended WCM for higher order interactions can be obtained by adding these higher order contributions to the Equations (5-2) as

$$\sigma_{for}^{\circ} = (1 - \eta)\sigma_{gr}^{\circ} + \eta\sigma_{gr}^{\circ} T_{tree} + \eta\sigma_{veg}^{\circ} (1 - T_{tree}) + (1 - \eta)\sigma_{gs}^{\circ} + \eta\sigma_{gs}^{\circ} T_{tree} \quad (5-11)$$

Highlighting the scattering from vegetation, surface and double-bounces and expressing the two-way tree transmissivity as the inverse of exponential product of attenuation per meter  $\alpha$  and thickness of the attenuating layer “ $h$ ” i.e.,  $T_{tree} = e^{-\alpha h}$ , the Equation (5-11) can be written as

$$\sigma_{for}^{\circ} = \sigma_{gr}^{\circ} \left( (1 - \eta) + \eta e^{-\alpha h} \right) + \eta \sigma_{veg}^{\circ} (1 - e^{-\alpha h}) + \eta \sigma_{gs}^{\circ} (1 - \eta + \eta e^{-\alpha h}) \quad (5-12)$$

So, the Equation (5-12) can be arranged in the two-way forest transmissivity using the Equation (5-5) by substituting

$$T_{for} = [1 - \eta + \eta e^{-\alpha h}]$$

The final equation for the extended water cloud model is presented as

$$\sigma_{for}^{\circ} = \sigma_{gr}^{\circ} T_{for} + \sigma_{veg}^{\circ} (1 - T_{for}) + \sigma_{gs}^{\circ} T_{for} \quad (5-13)$$

The Equation (5-13) can be written in the terms stem volume by expressing the two-way forest transmissivity in terms of stem volume  $v$  and empirically defined coefficient  $\beta$  by using the Equation (5-7) as

$$\sigma_{for}^{\circ} = \sigma_{gr}^{\circ} e^{-\beta v} + \sigma_{veg}^{\circ} (1 - e^{-\beta v}) + \sigma_{gs}^{\circ} e^{-\beta v} \quad (5-14)$$

### 5.3. Using polarimetric SAR for extended water cloud modelling:

The unknown parameters of the extended water cloud model, which can be observed from the Equation (5-14) are the backscattering from ground i.e.,  $\sigma_{gr}^{\circ}$ , the backscattering from the vegetation i.e.,  $\sigma_{veg}^{\circ}$  and the backscattering due to the stem ground interaction i.e.,  $\sigma_{gs}^{\circ}$  and the empirically defined coefficient  $\beta$ . In order to reduce the number of unknowns and to further simplify the model the polarimetric decomposition components are used. The ground backscattering term which represents the scattering from the bare ground and also from the ground visible through the canopy gaps are modelled using the surface scattering component from the decomposition. The backscattering from the vegetation which is obtained from the canopy is modelled using the volume scattering component. The ground and stem interaction term is modelled using the double-bounce scattering obtained from the decomposition. The total backscattering from the forest which represents the total power is received using the sum of all the decomposition components.

This reduces the number of unknowns to one i.e., the empirically defined coefficient  $\beta$ , which will be estimated separately for the modelling of stem volume and AGB. The model based decomposition described in the section 4.4.3 is generalized for different kinds of distributed targets. The use of these scattering components derived from this polarimetric decomposition for

modelling approach of extended WCM makes it applicable for parameter estimation of different types of vegetation. The addition of the ground stem interaction term to the water cloud model makes it applicable to the multi-layer vegetation where the layers are canopy, stem and ground.

So, the Equation (5-13) representing the extended water cloud model in the terms of decomposition components i.e., surface scattering, volume scattering and double-bounces scattering using the Equations (4-12), (4-13) and (4-14) can be written as

$$P = P_s T_{for} + P_v (1 - T_{for}) + P_d T_{for} \quad (5-15)$$

Here,

$P$  is the total power representing the total forest backscattering  $\sigma_{for}^{\circ}$

$P_s$  is the surface scattering representing the direct backscattering from ground  $\sigma_{gr}^{\circ}$

$P_d$  is the double-bounce scattering representing the backscattering from the ground stem interaction  $\sigma_{gs}^{\circ}$

The Equation (5-15) can be written in the terms of stem volume and  $\beta$  as

$$P = P_s e^{-\beta v} + P_v (1 - e^{-\beta v}) + P_d e^{-\beta v} \quad (5-16)$$

The above equation which is in the terms of stem volume,  $\beta$  and the respective scattering powers of surface, volume and double-bounce can be further inverted to obtain a relation between the *in-situ* measurements and PolSAR data.

## 6. RESULTS AND DISCUSSIONS:

The results obtained from the methods discussed in Chapter 4 and Chapter 5 are presented here. In the first and sections results and analysis for the OA shift and effect of deorientation on the decomposition components are discussed. In the third section parameter inversion estimation for the WCM using the PolSAR data are discussed. In the third section, results of parameter estimation for the extended water cloud model are presented. Modeling of stem volume and AGB are discussed in the section 4 and section 5 respectively along with the analysis on the accuracy assessment of the estimates. The discussions on the present research and the possible limitations with the review of methods adopted is presented in the last section

### 6.1. Orientation angle shift:

The orientation angle is estimated using the Equation (4-17) and the coherency matrix is deoriented using the Equation (4-18). The Figure (6-1) shows the estimated orientation angle shift image in the study area (Dudhwa National Park) and its histogram.

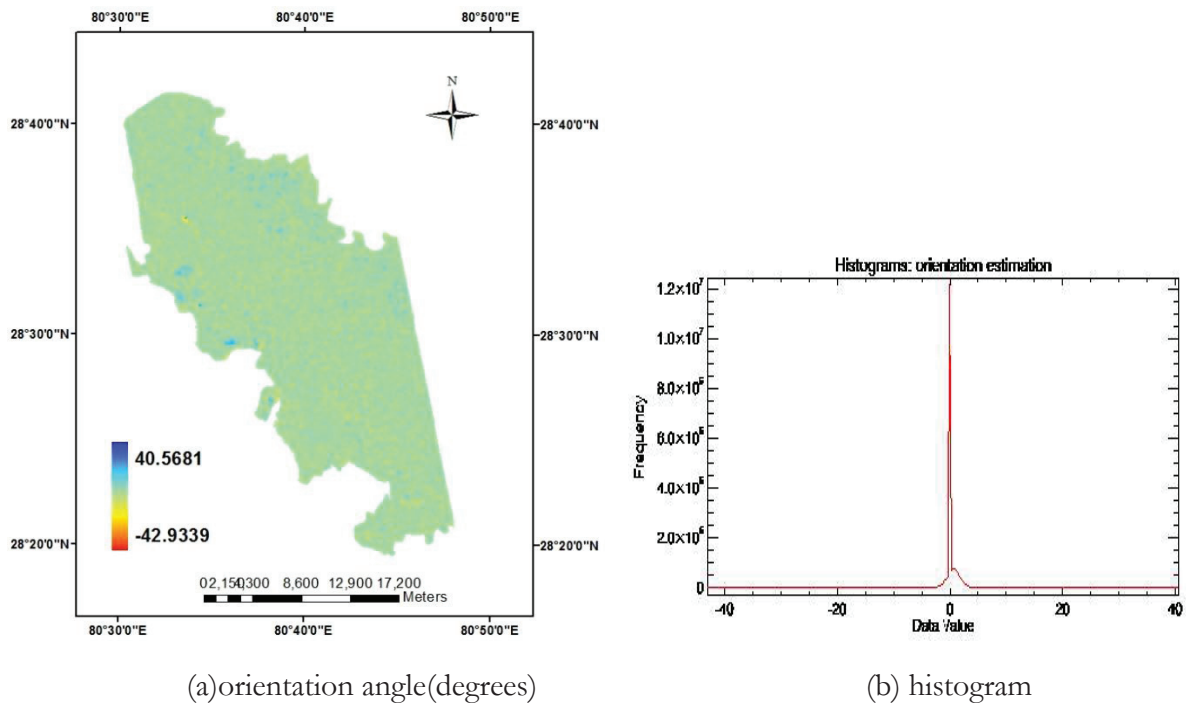


Figure 6-1 : (a) Estimated orientation angle shift image and (b) Histogram of the image

The Figure (6-1) (a) shows the estimated orientation angle shift image in degrees and (b) shows the histogram of the image. The estimated orientation angle shift lies in between the  $-45^{\circ}$  to  $+45^{\circ}$  is the anticipated value for this parameter using the Equation (4-17). This suggests that the data consist of OA shifts and needs to be compensated.

## 6.2. Effect of OA shift compensation on the decomposition components:

The deorientation on the coherency matrix is applied using the Equation (4-18) which rotates the coherency matrix along the line of sight using the estimated OA from Equation (4-17). The deorientation reduces the cross-polarized return T33 of the coherency matrix [28] [13] which is the responsible for the volume scattering component. The T22 element of the coherency matrix which is used in the modeling of double bounce scattering remains same or increases [28] [13]. The T11 element of the coherency matrix which is used in the modeling of surface scattering remains same after the deorientation in order to maintain the span.

### 6.2.1. Volume scattering:

The effects of OA shifts compensation have been studied on the results obtained from the Yamaguchi decomposition [12]. The deorientation is applied on the coherency matrix using the Equation (4-18) and later the deorientated coherency matrix is used for the decomposition. The results obtained from the decomposition before and after deorientation were analyzed for the volume scattering component which is mainly observed due to the backscattering from tree canopies in the forest areas.

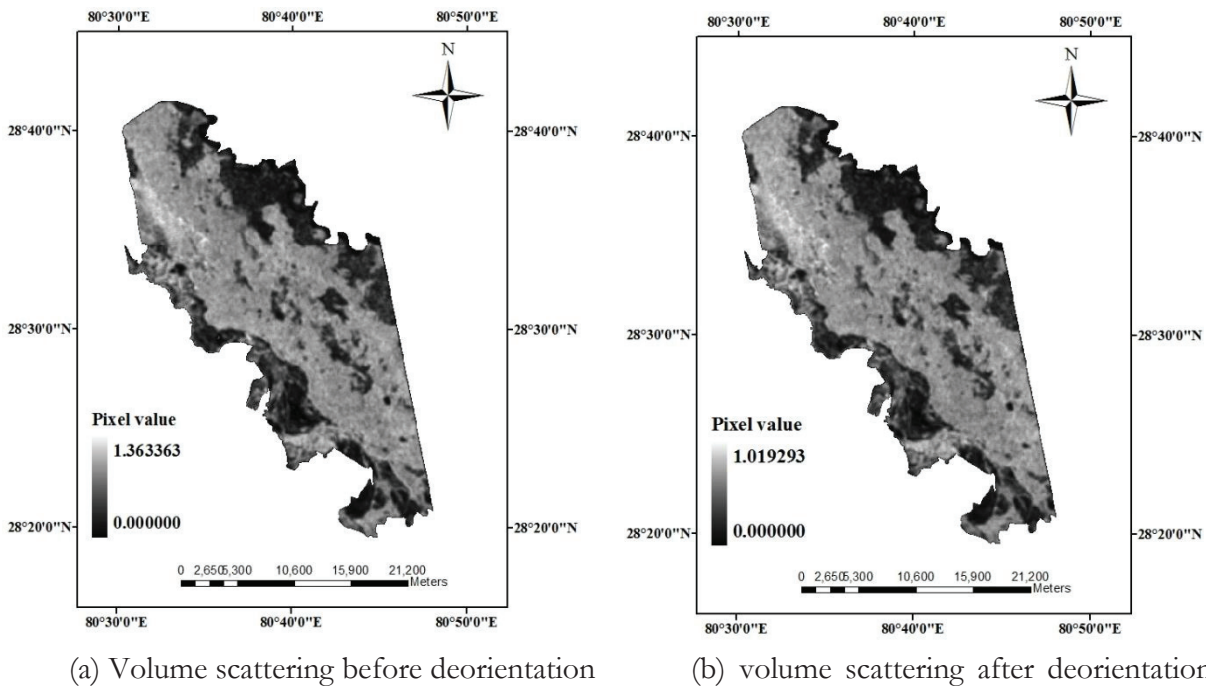


Figure 6-2 : Images showing the volume scattering components before and after deorientation.

Left and right images are before and after compensation results of volume scattering

The Figure (6-2) shows the images of the volume scattering components obtained before and after OA shifts compensation in the present study area (Dudhwa National Park). There has been a decrease in the volume scattering values when deorientation was applied. The deorientation reduces the cross-polarized  $T33 = 4(|S_{HV}|^2)$  element of the coherency matrix. There is a

decrease in the volume scattering component which is modeled using the T33 element of the coherency matrix. In order to analyze the deorientation effect on the volume scattering the plot level analyses on the deorientation of the volume scattering are analyzed using 152 points which were taken from the *in-situ* measurements.

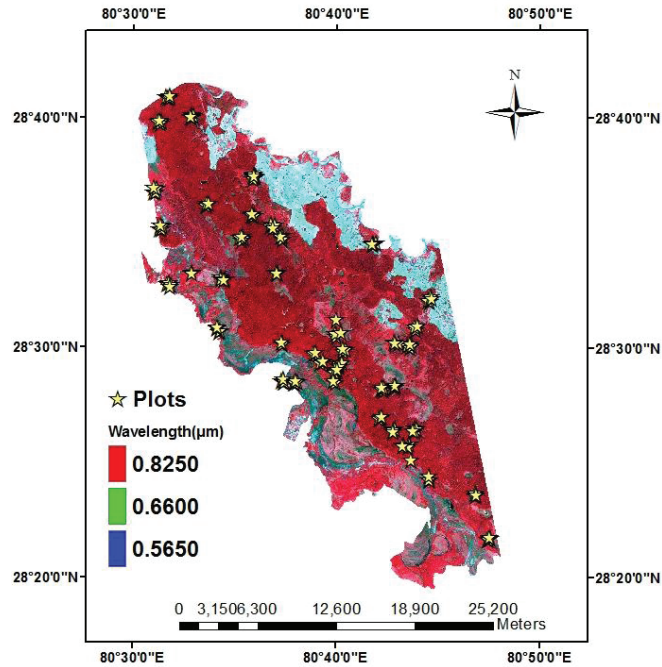


Figure 6-3 : ETM+ FCC image showing the plots selected for the analysis

The Figure (6-3) shows the ETM+ FCC with wavelengths ( $\mu\text{m}$ ) shown in Red – 0.8250 (NIR), Green- 0.6600 (Red) and Blue – 0.5650 (Green) band- image with points collected from the *in-situ* measurements shown in yellow stars. For the analysis of the changes in the volume scattering component, 152 points from the *in-situ* measurements are selected. These points are distributed over the study area and are selected from the two images of the volume scattering component before and after deorientation. The Figure (6-4) shows the volume scattering component before and after deorientation.

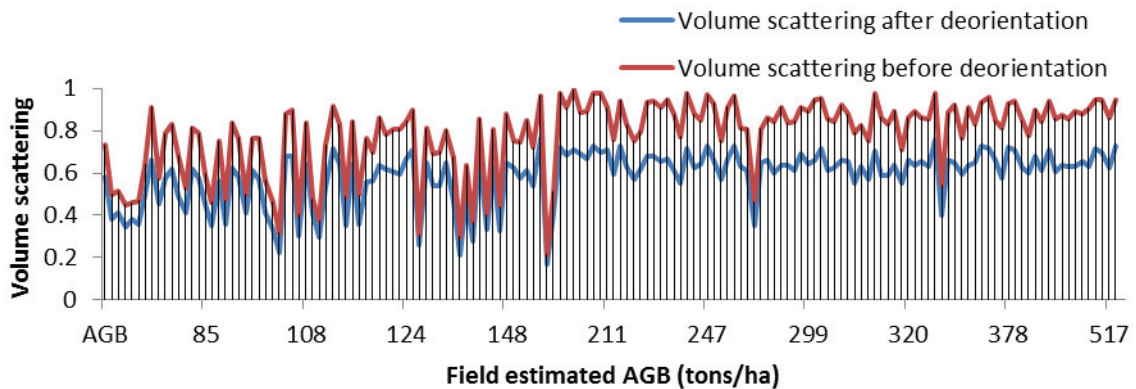


Figure 6-4 : Volume scattering before and after deorientation

In the Figure (6-4) the volume scattering after deorientation is displayed in blue line and volume scattering before deorientation is displayed in red line. The volume scattering before and after values are plotted against the ground measured AGB. Over estimation of volume scattering was reduced when deorientation was applied which is indicated by the change in the blue line with respect to the red line. Major decrease is observed in volume scattering for the plots in the dense forest areas with high biomass values. This shows that the over estimation in the volume scattering from the denser canopy is reduced after deorientation.

### 6.2.2. Double-bounce scattering:

The T22 element of the coherency matrix increases or remains the same after deorientation [28]. So, an increase in the double-scattering power is observed after deorientation which is modeled using the T22 element of the coherency matrix using the Equation (4-9). To analyze the effect of deorientation on the double-bounce scattering, 152 point from the *in-situ* measurements were used. These points are shown in the Figure (6-3).

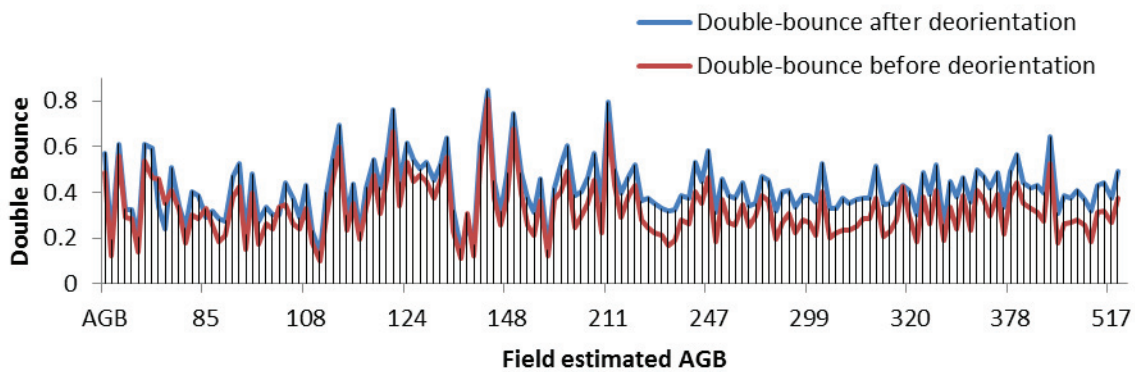


Figure 6-5 : Double-bounce scattering before and after deorientation

The values of double-bounce scattering before and after deorientation are plotted which is shown in the Figure 6-5. The blue line shows the double-bounce scattering values after deorientation and the values before deorientation are shown in red line. Increase in the blue line is observed with respect to the red line which implies that the double-bounce scattering is increased. Applying deorientation makes more accurate assessment of scattering components as double-scattering was expected from the forests due to the stem and ground returns when using longer wave lengths like L-band.

### 6.2.3. Surface scattering:

The T11 element of the coherency matrix remains same after the deorientation. From the Equation (4-18) it can be observed that the T11 element is roll-invariant to any orientation angle shifts and doesn't show any change when deorientation is applied [28]. The T11 element of the coherency matrix represents the surface scattering mechanism. The surface scattering component which is modeled using the T11 element showed an increase in the values when deorientation

was applied. To analyze the effect of deorientation on the surface scattering component 152 point from the *in-situ* measurements were taken which is shown in the Figure 6-3.

The points were collected from the surface scattering component before and after deorientation are plotted.

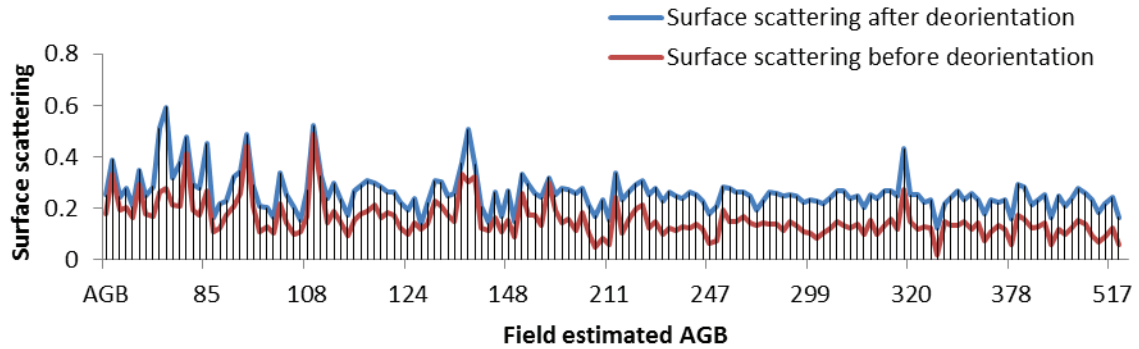


Figure 6-6 : Surface scattering before and after deorientation

The Figure (6-6) shows the plot of the points selected from the surface scattering before and after deorientation. The blue line represents the surface scattering values after deorientation and red line represents the surface scattering before deorientation. There is an increase in the blue line with respect to the red line which indicates the increase in the surface scattering after deorientation. Even though the T11 element is roll invariant, increase in the surface scattering is observed after deorientation. The modeling of surface scattering which includes other elements along with the T11 is the reason for the reduction in the values (Equation (4-11)).

### 6.3. Extended Water cloud model parameter estimation and results:

#### 6.3.1. Parameter estimation of extended water cloud model using PolSAR data:

The unknown parameters of the extended water cloud model are the total forest backscattering  $\sigma_{for}^{\circ}$ , the backscattering from vegetation layer  $\sigma_{veg}^{\circ}$ , backscattering from the ground  $\sigma_{gr}^{\circ}$ , backscattering from the interactions of ground and stem  $\sigma_{gs}^{\circ}$  and the empirically defined coefficient  $\beta$ . As discussed in the section 5.3, the use of polarimetric decomposition components reduces the unknown parameters to one i.e., empirically defined coefficient  $\beta$ .  $\beta$  is estimated using the *in-situ* measurements in the study area.

The extended water cloud model is trained for the estimation of  $\beta$  using the *in-situ* measurements for the 39 site clusters consisting of 152 plots which were collected in the Dudhwa National Park area in 2008. Selecting equal number plots from each cluster and half the total number of total plots are selected for training. Total 75 plots are selected for the estimation of  $\beta$ , an average value

of  $\beta$  is used in the modeling of which is estimated separately for the stem volume and AGB. The modeling of stem volume and AGB is done on the remaining plots.

The following steps are used in the unknown parameter estimation using the fully polarimetric ALOS-PALSAR L-band data.

- a) Decomposition of the fully polarimetric data. The decomposition is applied on the coherency matrix before and after deorientation. The results of decomposition before and after deorientation are used separately for estimation of the unknown parameter i.e.,  $\beta$ .
- b) Estimation of  $\beta$  for stem volume from the decomposition components obtained before and after deorientation.
- c) Estimation of  $\beta$  for AGB from the decomposition components obtained before and after deorientation.
- d) Modeling of stem volume and AGB using the  $\beta$  estimated for before and after deorientation.

### 6.3.2. Retrieval of $\beta$ for stem volume:

The parameters of the extended water cloud model are retrieved using the PolSAR data. The PolSAR data is decomposed in to volume scattering, surface scattering and double-scattering. The points collected in *in-situ* measurements are identified and collected extracted from these decomposition components. As discussed in the section 6.3.1 half the points are retained for  $\beta$  estimation and the remaining are used for modelling of stem volume.

The Equation (5-14) which relates the total forest backscatter and the scattering components and the *in-situ* measurements can be further inverted to obtained relation between  $\beta$  and backscattering components as

$$\beta_v = \frac{-1}{v} \left[ \ln \left( \frac{\sigma_{for}^o - \sigma_{veg}^o}{\sigma_{gr} - \sigma_{veg} + \sigma_{gs}} \right) \right] \quad (6-1)$$

The  $\beta_v$  values are estimated for the selected plots using the scattering components before and after deorientation.

$$\frac{\sum_{i=1}^N \beta_{v-before}}{N} = \frac{\sum_{i=1}^N \left[ \frac{-1}{v} \left[ \ln \left( \frac{\sigma_{for}^o - \sigma_{veg}^o}{\sigma_{gr} - \sigma_{veg} + \sigma_{gs}} \right) \right] \right]}{N} \quad (6-2)$$

$$\frac{\sum_{i=1}^N \beta_{v-after}}{N} = \frac{\sum_{i=1}^N \left[ \frac{-1}{v} \left[ \ln \left( \frac{\sigma_{for}^o - \sigma_{veg}^o}{\sigma_{gr} - \sigma_{veg} + \sigma_{gs}} \right) \right] \right]}{N} \quad (6-3)$$

Here,

$\beta_{v-before}$  and  $\beta_{v-after}$  are the  $\beta_v$  values estimated from the decomposition components before and after deorientation respectively for stem volume.

$N$  is the number of plots used for the estimation ( here  $N = 75$  )

As the Equations(6-2), (6-3) are divided by the number of plots  $N$ , we get an average of  $\beta$  for the plots the plots used for its estimation.

Table 6-1: Estimated  $\beta_v$  values for the modelling of stem volume

Stem volume	$\beta_v$ (ha/m <sup>3</sup> )	
	Before deorientation ( $\beta_{v-before}$ )	After deorientation ( $\beta_{v-after}$ )
	0.004333	0.004713

Table (6-1) gives the details of the estimated  $\beta_v$  values estimated using the Equation (6-2) and Equation (6-3) for the modelling of stem volume. The  $\beta_v$  value is kept constant for the modelling of stem volume on the remaining plots. As Equation (6-1) consist of two types of input quantities; the unit less backscattering values from forest, vegetation, surface and stem ground interactions and the stem volume with unit m<sup>3</sup>/ha obtained from the *in-situ* measurements. The  $\beta_v$  obtains the unit of inverse of the stem volume i.e., ha/m<sup>3</sup>.

#### 6.4. Retrieval of stem volume:

The stem volume is retrieved by inverting the extended water cloud model. The inversion is done using the remaining 77 plots which are not used for the parameter estimation and using the  $\beta_v$  values estimated. The  $\beta_v$  given in the Table (6-1) were used for the modelling of stem volume before and after deorientation. The formula used for the estimation of stem volume is obtained using the Equation (5-14) which relates the scattering components and the  $\beta_v$  value estimated for the modelling of stem volume.

$$v_{before} = \frac{-1}{\beta} \left[ \ln \left( \frac{\sigma_{for}^i - \sigma_{veg}^i}{\sigma_{gr} - \sigma_{veg} + \sigma_{gs}} \right) \right] \quad (6-4)$$

$$v_{after} = \frac{-1}{\beta} \left[ \ln \left( \frac{\sigma_{for}^i - \sigma_{veg}^i}{\sigma_{gr} - \sigma_{veg} + \sigma_{gs}} \right) \right] \quad (6-5)$$

Here,

$v_{before}$  is the stem volume estimated using the components before deorientation

$v_{after}$  is the stem volume estimated using the components after deorientation.

Scatterplot is plotted between the modeled stem volume and the field estimated stem volume. Figure (6-7) shows the relationship between the modeled stem volume and the field estimated stem volume. The scatterplot (a) shows the relationship between the modeled stem volume before deorientation and the field estimated stem volume. The scatterplot (b) shows the modeled stem volume after deorientation. In both the plots the modeled stem volume suffered the saturation problem.

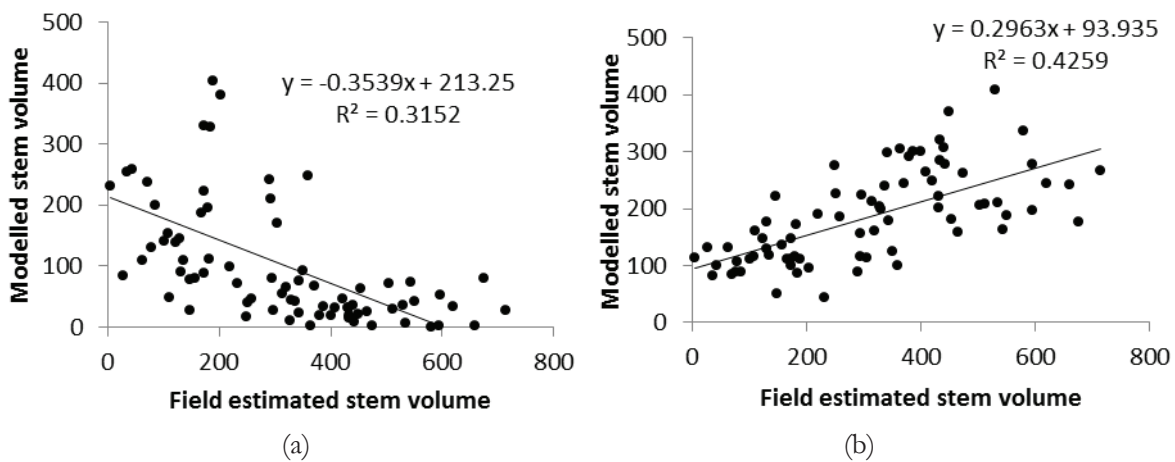


Figure 6-7 : Plot showing the relationship between the field estimated stem volume and the modelled stem volume (a) before deorientation (b) after deorientation

The best fit straight line through these points in the scatterplot shows that correlation between the modeled stem volume and the field estimated stem volume. The correlation of the after deorientation stem volume is acceptable while the before deorientation stem volume is showing a negative slope where a positive correlation between field estimated stem volume and modeled stem volume is expected. The coefficient of determination (R-square) which shows the closeness of the estimated values with the measured values is used to show the correlation of the modeled stem volume with the field estimated stem volume. For the before deorientation stem volume, a correlation of 0.3152 is obtained. For the after deorientation stem volume a correlation of 0.4259 is observed with the field estimated stem volume. The after deorientation stem volume is well correlated with field estimated stem volume, but some over estimation and under estimation of the stem volume is also observed. The noise present in the data is a reason for this along with the saturation problem. The need to compensate the OA shifts by the deorientation of the PolSAR data before relating to the stem volume is observed from the results.

In order to assess the error in the modeled stem volume another statistical method was implemented which is root mean square error or RMSE. The RMSE is calculated for the modeled stem volume and field estimated stem volume using the formula

$$RMSE = \sqrt{\frac{\sum_{i=1}^N (Volume_{measured} - Volume_{estimated})^2}{N}} \quad (6-6)$$

Here ,

$Volume_{measured}$  is the field estimated stem volume

$Volume_{estimated}$  is the model estimated stem volume

$N$  is the number of plots used in the modeling (here  $N = 77$ )

Table 6-2 :  $\beta$ , RMSE and R-square obtained for modelled stem volume before and after deorientation

Modelled stem volume	Before deorientation			After deorientation		
	$\beta$ (ha/m <sup>3</sup> )	RMSE	R-square	$\beta$ (ha/m <sup>3</sup> )	RMSE	R-Square
	0.004333	328.99	0.3152	0.004713	185.904	0.4259

Table (6-2) showcases the  $\beta$ , RMSE and R-square obtained from the modelling of stem volume using the extended water cloud model. It is clear from the Table (6-2) that a reasonable R-square value and low RMSE is obtained for the after deorientation stem volume when compared to the before deorientation stem volume. This show that the PolSAR data needs to be compensated for OA shifts. Analysis is done on the RMSE for the plots with field estimated stem volume less than 300 m<sup>3</sup>/ha and above 300 m<sup>3</sup>/ha. Out of 77 plots used for the modelling of AGB, 37 plots having the field estimated stem volume <300 tons/ha and 40 plots with field estimated stem volume > 300 tons/ha are identified and RMSE for these plots were calculated. The obtained RMSE's are provided in the Table (6-5).

Table 6-3 : RMSE obtained for the plots with field estimated stem volume < 300 m<sup>3</sup>/ha

Modelled stem volume	Before deorientation		After deorientation	
	Filed estimated stem volume <300 m <sup>3</sup> /ha	Field estimated stem volume >300 m <sup>3</sup> /ha	Field estimated stem volume <300 m <sup>3</sup> /ha	Field estimated stem volume >300 m <sup>3</sup> /ha
	RMSE (m <sup>3</sup> /ha)			
	161.876	429.099	80.5779	246.013

Table (6-3) showcases the RMSE obtained for the plots having the field estimated stem volume values less than 300 m<sup>3</sup>/ha and greater than 300 m<sup>3</sup>/ha. From the table it is clear that the RMSE is less for the plots with the field estimated stem volume <300 m<sup>3</sup>/ha when compared to those plots with field estimated stem volume >300 m<sup>3</sup>/ha. The after deorientation stem volume for the plots with field estimated stem volume <300 m<sup>3</sup>/ha is much more accurate with a RMSE of 80.57 m<sup>3</sup>/ha. It is low when compared to the combined RMSE obtained in the Table (6-2). The combined RMSE obtained in the Table (6-2) is high which is due to the error induced by the plots with field estimated AGB > 300 tons/ha which is due to the saturation problem.

### 6.5. Modeling of AGB from PolSAR data:

Modeling of AGB is done using the extended water cloud model which is similar to that of used in the modeling of stem volume. The equation for the modeling of AGB is as follows.

$$\sigma_{for}^{\circ} = \sigma_{gr}^{\circ} e^{-\beta B} + \sigma_{veg}^{\circ} (1 - e^{-\beta B}) + \sigma_{gs}^{\circ} e^{-\beta B} \quad (6-7)$$

Here,

$B$  is the above ground biomass.

The Equation (6-7) relates the scattering components- surface scattering  $\sigma_{gr}^{\circ}$ , volume scattering  $\sigma_{veg}^{\circ}$ , double-bounce scattering  $\sigma_{gs}^{\circ}$ , total power  $\sigma_{for}^{\circ}$  and the AGB and the empirically defined coefficient  $\beta$ . This equation is further inverted for the estimation of the unknown parameter  $\beta$  using the *in-situ* measurements.

#### 6.5.1. Retrieval of $\beta$ for AGB:

$\beta$  for AGB modelling will be estimated similar to that of the stem volume. The same plots selected for the modelling of stem volume are used in the estimation of  $\beta$ . By inverting the Equation (6-7) for the estimation  $\beta$  we get the following relation as

$$\beta_B = \frac{-1}{B} \left[ \ln \left( \frac{\sigma_{for}^{\circ} - \sigma_{veg}^{\circ}}{\sigma_{gr}^{\circ} - \sigma_{veg}^{\circ} + \sigma_{gs}^{\circ}} \right) \right] \quad (6-8)$$

The  $\beta_B$  value was estimated using the decomposition components before and after deorientation and the field estimated AGB from the selected plots.

$$\frac{\sum_{i=1}^N \beta_{B-before}}{N} = \frac{\sum_{i=1}^N \left[ \frac{-1}{B} \left[ \ln \left( \frac{\sigma_{for}^{\circ} - \sigma_{veg}^{\circ}}{\sigma_{gr}^{\circ} - \sigma_{veg}^{\circ} + \sigma_{gs}^{\circ}} \right) \right] \right]}{N} \quad (6-9)$$

$$\frac{\sum_{i=1}^N \beta_{B-after}}{N} = \frac{\sum_{i=1}^N \left[ \frac{-1}{B} \left[ \ln \left( \frac{\sigma_{for}^{\circ} - \sigma_{veg}^{\circ}}{\sigma_{gr}^{\circ} - \sigma_{veg}^{\circ} + \sigma_{gs}^{\circ}} \right) \right] \right]}{N} \quad (6-10)$$

Here,  $\beta_{B-before}$ ,  $\beta_{B-after}$  are the  $\beta_B$  values obtained using the before and after deorientation decomposition components respectively.

$B$  is the field estimated AGB which is used in the estimation  $\beta_{B-before}$ ,  $\beta_{B-after}$  for the selected plots.

$N$  is the number of plots selected for parameter estimation. (here  $N = 75$ )

Table 6-4 : Estimated  $\beta_B$  values for the modelling of AGB

AGB	$\beta_B$ (ha/tons)	
	Before deorientation ( $\beta_{B-before}$ )	After deorientation ( $\beta_{B-after}$ )
	0.004617	0.005897

Table (6-4) gives the details of the estimated  $\beta$  values using the Equations (6-9) and(6-10). The  $\beta$  value is kept constant for the modelling of AGB on the remaining plots. The Equation (6-8) consist of unit less backscattering values from forest, volume scattering from vegetation, surface scattering from ground, double-bounce scattering from ground stem interaction and ground estimated AGB with units tons/ha. The  $\beta_B$  obtains the unit of inverse of ABG i.e., ha/tons.

### 6.5.2. Retrieval of AGB:

The AGB is modeled by inverting the extended water cloud model. The inversion is done using the remaining plots which are not used for the parameter estimation and using the  $\beta_B$  values estimated. The  $\beta_B$  given in the Table (6-4) are used for the modelling of stem volume before and after deorientation. The formula used for the estimation of AGB is obtained by inverting the Equation(6-7) which relates the scattering components and the  $\beta_B$  value estimated for the modelling of AGB.

$$B_{before} = \frac{-1}{\beta} \left[ \ln \left( \frac{\sigma_{for}^0 - \sigma_{veg}^0}{\sigma_{gr} - \sigma_{veg} + \sigma_{gs}} \right) \right] \quad (6-11)$$

$$B_{after} = \frac{-1}{\beta} \left[ \ln \left( \frac{\sigma_{for}^0 - \sigma_{veg}^0}{\sigma_{gr} - \sigma_{veg} + \sigma_{gs}} \right) \right] \quad (6-12)$$

Here,

$B_{before}$  is the modelled AGB using the decomposition components before deorientation and

$B_{after}$  is the modelled AGB using the decomposition components after deorientation

The following scatterplots are obtained using the field estimated AGB and modelled AGB before and after deorientation and the field estimated AGB.

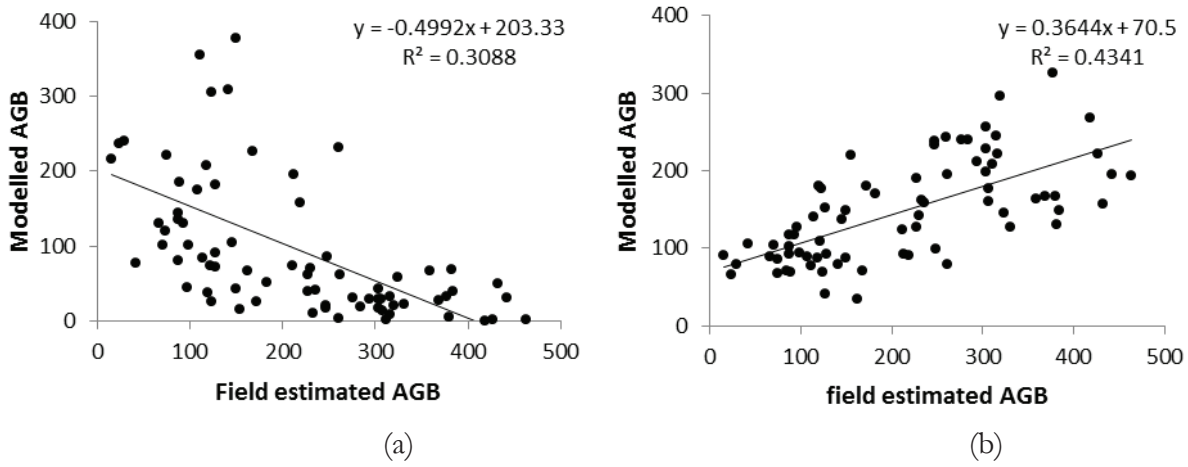


Figure 6-8 : Plot showing the relationship between the field estimated AGB and the modelled AGB (a) before deorientation (b) after deorientation

Figure (6-8) show the relationship of modelled AGB and field estimated AGB. The scatterplot (a) show the relationship of before deorientation AGB and the field estimated AGB. The scatterplot (b) show the relationship between the after deorientation AGB and the field estimated AGB.

The best fit line through the points in the scatterplot show the correlation of the modelled AGB and field estimated AGB. The after deorientation AGB is showing a good correlation while the before deorientation AGB is having a negative slope. The coefficient of determination (R-square) for before deorientation AGB is 0.3088 and for the after deorientation AGB 0.4341 is obtained. The after deorientation AGB is correlated better with the field estimated AGB when compared to the before deorientation AGB. The after and before deorientation AGB's suffered saturation problem. It is observed from the scatterplots that for some field estimated low AGB plots are overestimated and high field measured AGB plots are under estimated. This is due to the saturation problem and also the noise present in the data. Overestimation and underestimation is low in the case of after deorientation AGB when compared to the before deorientation AGB, which shows that the deorientation reduces the erroneous results when the PolSAR data is related to the AGB. From the Figure (6-8) it is evident that the extended water model predicted the AGB with the reasonable correlation when deorientation is applied.

RMSE is also calculated for both after and before deorientated AGB with respect to the field is measured AGB using the formula

$$RMSE = \sqrt{\frac{\sum_{i=1}^N (AGB_{measured} - AGB_{estimated})^2}{N}} \tag{6-13}$$

Here ,

$AGB_{measured}$  is the field estimated AGB,  $AGB_{estimated}$  is the model estimated AGB

$N$  is the number of plots used in the modeling (here  $N = 77$ )

Table 6-5:  $\beta$ , RMSE and R-square obtained for modelled AGB before and after deorientation

Modelled AGB	Before deorientation			After deorientation		
	$\beta$ (ha/tons)	RMSE (tons/ha)	R-square	$\beta$ (ha/tons)	RMSE (tons/ha)	R-Square
	0.004617	234.39	0.3088	0.005897	119.59	0.4341

The Table (6-5) showcases the  $\beta$  used for the modelling of AGB, RMSE and coefficient of determination obtained for the before and after deorientation AGB. Low RMSE and better correlation (R-square) is obtained for the after deorientation AGB when compared to the before deorientation AGB. The RMSE is observed to be large in both before and after deorientation AGB and it is observed that the field estimated AGB for some plots are having values less than the obtained RMSE. So, an analysis is on the RMSE for the plots with field estimated AGB values less than 300 tons/ha and above 300 tons/ha. Out of 77 plots used for the modelling of AGB, 53 plots having the field estimated AGB <300 tons/ha and 24 plots with field estimated AGB > 300 tons/ha are identified and RMSE for these plots were calculated. The obtained RMSE's are provided in the Table (6-5).

Table 6-6 : RMSE obtained for the plots with field estimated AGB < 300 tons/ha

Modelled AGB	Before deorientation		After deorientation	
	Field estimated AGB <300 tons/ha	Field estimated AGB >300 tons/ha	Field estimated AGB <300 tons/ha	Field estimated AGB >300 tons/ha
	RMSE (tons/ha)	RMSE (tons/ha)	RMSE (tons/ha)	RMSE (tons/ha)
	159.42	346.60	64.12	191.86

The Table (6-6) showcases the RMSE obtained for the plots having the field estimated AGB values less than 300 tons/ha and greater than 300 tons/ha. From the table it is clear that the RMSE is less for the plots with the field estimated AGB <300 tons/ha when compared to those plots with field estimated AGB>300 tons/ha. The after deorientation AGB for the plots with field estimated AGB <300 tons/ha is much more accurate with a very low RMSE of 64.12 tons/ha. It is low when compared to the combined RMSE obtained in the Table (6-5). The combined RMSE obtained in the Table (6-5) is high which is due to the error induced by the plots with field estimated AGB > 300 tons/ha which is due to the saturation problem.

As better correlation and low RMSE was obtained for the deorientation AGB, its accuracy is evaluated using the following formula [60].

$$\text{Accuracy (\%)} = 1 - \frac{1}{N} \sum_{i=1}^N \frac{(AGB_{measured} - AGB_{estimated})}{AGB_{estimated}} \times 100 \quad (6-14)$$

Here,  $AGB_{measured}$  is the modeled AGB,  $AGB_{estimated}$  is the field estimated AGB and  $N$  is the number of plots used for the modelling of biomass ( $N = 77$ ). 56 % accuracy is obtained for the modelled AGB after deorientation using the Equation(6-14).

## 6.6. Discussions:

The present research is focused on the estimation of biophysical parameters using the PolSAR data decomposition components. The effect of OA shift on the PolSAR data is reduced by deorientating the coherency matrix. Previous research has shown that the PolSAR data is affected by the OA shift caused by the terrain and the orientation of the targets to the radar line of sight. These shifts increase the cross polarized intensity which results in the overestimation of volume scattering. In this research the orientation angle shift is estimated and the coherency matrix is deorientated to compensate the shifts. The deorientation has reduced the volume scattering and increased the double bounce scattering. From the Figure 6-4 it is observed that decrease in the volume scattering is more in the plots with more AGB. The volume scattering is observed to increase with the increase in the AGB up to a certain saturation limit in both the after and before deorientation. No particular trend is observed in the double bounce scattering for both before and after deorientation when observed the Figure 6-5. The surface scattering is also increased when deorientation is applied when deorientation is applied which is observed from the Figure 6-6. It is observed that the decrease in the in the volume scattering is not equal to the increase to increase in the double bounce scattering or the surface scattering. The decrease in the volume scattering and the increase in the surface scattering after the deorientation tend to stabilize in the same AGB range of 210-240 tons/ha and a particular trend is not observed for the double bounce scattering. The differences in the canopy thickness for different plots and the orientation of the trees to the radar line of sight could also affect the deorientation which indeed affects the scattering mechanisms.

Another objective of this research is to extend the semi-empirical water cloud model for higher order interactions from the ground and stem interactions. This is realized by utilizing the previously developed water cloud model including gaps and the decomposition components, which is explained in the Chapter 5. The parameter estimation of the extended water cloud model with the help of decomposition components and the *in-situ* measurements and the modeling of the stem volume and AGB are discussed in the previous sections. The parameter  $\beta_v, \beta_E$  retrieved for the modeling of stem volume and AGB respectively are in specified range [17]. The stem volume and AGB are retrieved from the decomposition components and the parameter estimated which is explained in the previous sections.

The extended water cloud model using deoriented decomposition components retrieved stem volume with reasonable accuracies. The effect of deorientation is analysed on the modeled stem volume. The coefficient of determination for before deorientation stem volume is 0.315 with an RMSE of 328 m<sup>3</sup>/ha and for the after deorientation stem volume is 0.4259 with an RMSE of 185 m<sup>3</sup>/ha, even though the coefficient of determination in the acceptable range the RMSE is very high. The saturation of the PolSAR data could be one of the reasons for high RMSE. So, an analysis is done by selecting the plots with stem volume less than 300 m<sup>3</sup>/ha and greater than 300 m<sup>3</sup>/ha. The decrease in the RMSE is found in both before deorientation stem volume and after deorientation stem volume. This clearly shows error induced by the saturation as the plots with high field estimated stem volume are cause for high error. This can be observed from the Table 6-3. The effect of deorientation on the modeled stem volume is clearly observed from the Figure 6-7. The after deorientation stem volume is better correlated with the field estimated stem volume, the before deorientation stem volume is showing a negative slope. Reduce in the volume scattering and increase in the double bounce scattering and surface scattering improved the stem volume estimates. It is observed that the deorientation improved the saturation limit when compared to that of the before deorientation stem volume.

The description and analysis for the modeling of AGB is provided in the section 6.5. The extended water cloud model estimated the AGB with reasonable accuracies when the deoriented decomposition components are used. The effect of deorientation is analyzed on the model estimated AGB. The coefficient of determination of the before deorientation AGB is 0.3088 with RMSE 234.39 tons/ha and for after deorientation AGB is 0.4341 with RMSE 119.59 tons/ha. The obtained RMSE is very high for both before and after deorientation AGB. A similar kind of analysis for the RMSE is done to analyze the effect of saturation on the modeled AGB with the plots having the field estimated AGB less than 300 tons/ha and greater than 300 tons/ha which is presented in the Table 6-6. RMSE is found to be decreased for both after and the before deorientation AGB. This show that the error induced by the plots with high field estimated AGB similar to that of the modeled stem volume. Similar to that of the before deorientation stem volume, the before deorientation AGB has shown negative slope. The deorientation has improved the saturation limit when compared to that of the before deorientation AGB and the previous studies [61]. The PolSAR images acquired in the low incidence angle is also a reason for the improvement in the saturation limit along with the effect of deorientation.



## 7. CONCLUSIONS AND RECOMMENDATIONS:

This chapter provides the answers to the research questions formulated in the section 1.3 to achieve the objective of this study. As mentioned in the chapter 1 the prime objective of this study is to estimate the stem volume and above ground biomass of the multilayered vegetation from the PolSAR data using modeling approach. This is achieved by compensating the orientation angle shifts induced in the PolSAR data, decomposing PolSAR data for the retrieval various scattering mechanisms using a polarimetric decomposition model. Semi-empirical water cloud model is extended in order to use the higher order scattering information from the ground stem interactions. The semi-empirical extended water cloud model is used to relate the forest biophysical parameters and the scattering information obtained from the PolSAR data decomposition.

### 7.1 CONCLUSIONS:

a) Which scattering mechanism is better related to the field estimated stem volume and AGB?

The volume scattering component is better related to the field estimated stem volume and AGB. The volume scattering before deorientation and after deorientation have shown increasing trend with the increase in the field estimated AGB. The double bounce scattering and surface scattering showed no particular trend with the field estimates.

b) What is the effect of deorientation on the decomposition?

The deorientation reduced the volume scattering component of the decomposition. The deorientation reduced the cross polarized component which is used to model the volume scattering. The double bounce scattering is increased after the deorientation. The increase in the double bounce scattering is not equal to the decrease in the volume scattering. Increase in the surface scattering is also observed when deorientation is applied.

c) How can the WCM be extended to include higher order interactions?

The water cloud model is extended by adding an additional component which accounts for the higher order interactions like ground stem interactions. The previous water cloud model accounts only two types of scattering mechanisms which are the scattering from the vegetation and the scattering from the ground. Longer wavelengths like L-band penetrate more through the canopy and provide the information of the underlying stem and ground which is not included in the WCM. And when L-band is used the backscattering from the stem ground interactions are also obtained which needs to be included when the PolSAR data in L-band wavelength is related to the biophysical parameters of the forest. The Polarimetric decompositions are helpful in retrieving various scattering mechanisms and also used in extending the water cloud model.

Volume scattering is used to represent the backscattering from vegetation, surface scattering for backscattering and double bounce scattering for backscattering due to higher order interactions.

d) How can the parameters of the extended water cloud model be retrieved?

The parameters of the extended water cloud model are the total forest backscattering, backscattering from the vegetation, backscattering from the ground, backscattering from the ground stem interaction and the empirically defined coefficient  $\beta$ . The use of decomposition components reduces the number of unknowns to one i.e.,  $\beta$ . This unknown parameter  $\beta$  is estimated with the decomposition components along with the *in-situ* measurements. The parameter is estimated for the modeling of stem volume and AGB separately. For the parameter estimation, 75 plots out of 152 plots from the *in-situ* measurements are taken and along with the decomposition components and used to model stem volume and AGB for the remaining 77 plots.

e) How does the deorientation affect the estimated stem volume and AGB?

The decrease in the volume scattering and increase in the double bounce scattering and surface scattering after deorientation and use of these deoriented decomposition components in the modeling showed improvement in the modeled estimated of stem volume and AGB. Estimates of the modeled stem volume and AGB are found to be better correlated with the field estimated stem volume and AGB when deorientation is applied. It is observed that the decrease in the underestimation and overestimation of the retrieved stem volume and AGB when deorientation is applied when compared with that of the before deorientation stem volume and AGB.

f) What is the improvement on the estimated stem volume and AGB after OA shift compensation?

Improvement in the saturation limits of the retrieved stem volume and AGB is observed when deorientation is applied. It is observed that the deorientation stem volume and AGB are more correlated to the field estimated stem volume and AGB when compared to that of the before deorientation stem volume and AGB. The deorientation stem volume and AGB showed improved correlation with the field estimated stem volume and AGB as the before deorientation stem volume and AGB showed negative slope when related to the field estimated stem volume and AGB.

g) What is the accuracy of the modeled stem volume and AGB with respect to the field estimated stem volume and AGB?

The extended water cloud model modeled the stem volume with a coefficient of determination (R-square) for before deorientation stem volume 0.3152 which is less than the after deorientation

stem volume 0.4259. The RMSE obtained for the before deorientation stem volume is 328.99 m<sup>3</sup>/ha is greater than the after deorientation stem volume 185.904 m<sup>3</sup>/ha (Table 6-2). Low RMSE and high correlation is found in the modeled stem volume after deorientation. The plots with field estimated stem volume < 300 m<sup>3</sup>/ha showed low RMSE of 80.5779 m<sup>3</sup>/ha for the after deorientation stem volume (Table 6-3). In the modeling of AGB, the coefficient of determination obtained for before deorientation AGB is 0.3088 and less than the after deorientation AGB 0.4341. The RMSE obtained for the before deorientation AGB 234.39 tons/ha is greater than RMSE of after deorientation AGB 119.59 tons/ha. The plots with field estimated AGB < 300 tons/ha showed low RMSE of 64.12 tons/ha for the after deorientation AGB (Table 6-6).

## 7.2 RECOMMENDATIONS:

In this research the biophysical parameters are estimated using the extended water cloud model using the decomposition components and the *in-situ* measurements. The four component decomposition model was developed by assuming the non-reflection symmetry condition, but the model inherently uses the reflection symmetry condition and only six elements out of nine elements of the coherency matrix are used. The remaining elements are needed to include in the modeling as these elements also contain the backscattering information from the targets. The deorientation produced better results in the present study, but its efficiency should be tested on different datasets and on different areas. Different filtering techniques are to be analyzed which preserves the information and spatial resolution and reduces the speckle noise.

This modeling approach in the present study considered only three scattering mechanisms—scattering from vegetation, scattering from ground and scattering from ground stem interactions. Scattering from the canopy-ground and canopy-stem forward scattering is accounted in the present modeling approach, which can be considered for further research.

The modeling approach in the present study used the ALOS –PALSAR L-band quad pol data over dense tropical forest. The results obtained using the extended water cloud model for the modeling of stem volume and AGB show that the PolSAR data can be used for the estimation of forest biophysical parameters. The accuracy of the modeled stem volume and AGB using the present modeling approach used in this study are moderate. Multi-temporal data approach is needed to be tested for improving the accuracies of the estimates. This use of high temporal data in longer wavelengths combined with the present modeling approach can be considered for further research. The present study can be carried further by testing its applicability on different forest types and different climatic conditions.



## REFERENCES

- [1] Food And Agriculture Organization, *State of the world's forests 2012*. [S.l.]: Food & Agriculture Organization, 2012.
- [2] "The Forest Biome." [Online]. Available: <http://www.ucmp.berkeley.edu/glossary/gloss5/biome/forests.html>. [Accessed: 25-Jul-2012].
- [3] A. P. Kirilenko and R. A. Sedjo, "Climate change impacts on forestry," *PNAS*, vol. 104, no. 50, pp. 19697–19702, Dec. 2007.
- [4] M. Santoro, C. Beer, O. Cartus, C. Schmullius, A. Shvidenko, I. McCallum, U. Wegmueller, and A. Wiesmann, "Retrieval of growing stock volume in boreal forest using hyper-temporal series of Envisat ASAR ScanSAR backscatter measurements," *Remote Sensing of Environment*, vol. 115, no. 2, pp. 490–507, Feb. 2011.
- [5] S. Brown, *Estimating biomass and biomass change of tropical forests: a primer*, vol. 134. Food & Agriculture Organization, 1997.
- [6] D. P. Lusch, "Introduction to microwave remote sensing," *Center for Remote Sensing and Geographic Information Science Michigan State University*, 1999.
- [7] I. H. Woodhouse, *Introduction to microwave remote sensing*. Boca Raton: Taylor & Francis, 2006.
- [8] J. A. Richards, G.-Q. Sun, and D. S. Simonett, "L-Band Radar Backscatter Modeling of Forest Stands," *IEEE Transactions on Geoscience and Remote Sensing*, vol. GE-25, no. 4, pp. 487–498, Jul. 1987.
- [9] Canada Centre for Remote sensing, "Advanced Radar Polarimetry Tutorial." [Online]. Available: [www.nrcan.gc.ca/sites/www.nrcan.gc.ca.../polarim\\_e.pdf](http://www.nrcan.gc.ca/sites/www.nrcan.gc.ca.../polarim_e.pdf). [Accessed: 16-May-2012].
- [10] W.-M. Boerner and J.-S. Lee, "Review of existing monographs and books on radar polarimetry and polarimetric SAR with the aim of justifying the need of updates," in *Geoscience and Remote Sensing Symposium, 2007. IGARSS 2007. IEEE International, 2007*, pp. 180–183.
- [11] A. Freeman and S. L. Durden, "A three-component scattering model for polarimetric SAR data," *IEEE Transactions on Geoscience and Remote Sensing*, vol. 36, no. 3, pp. 963–973, May 1998.
- [12] Y. Yamaguchi, Y. Yajima, and H. Yamada, "A four-component decomposition of POLSAR images based on the coherency matrix," *IEEE Geoscience and Remote Sensing Letters*, vol. 3, no. 3, pp. 292–296, Jul. 2006.

- [13] J.-S. Lee and T. L. Ainsworth, "The Effect of Orientation Angle Compensation on Coherency Matrix and Polarimetric Target Decompositions," *IEEE Transactions on Geoscience and Remote Sensing*, vol. 49, no. 1, pp. 53–64, Jan. 2011.
- [14] E. Attema and F. Ulaby, "Vegetation Modeled as a Water Cloud," *Radio Science*, vol. 13, no. 2, pp. 357–364, 1978.
- [15] F. T. Ulaby, K. McDonald, K. Sarabandi, and M. C. Dobson, "Michigan Microwave Canopy Scattering Models (MIMICS)," in *Geoscience and Remote Sensing Symposium, 1988. IGARSS '88. Remote Sensing: Moving Toward the 21st Century, International*, 1988, vol. 2, p. 1009.
- [16] S. Kumar, U. Pandey, S. P. Kushwaha, R. S. Chatterjee, and W. Bijker, "Aboveground biomass estimation of tropical forest from Envisat advanced synthetic aperture radar data using modeling approach," *Journal of Applied Remote Sensing*, vol. 6, Oct. 2012.
- [17] M. Santoro, J. Askne, L. Eriksson, C. Schmullius, A. Wiesmann, and J. E. S. Fransson, "Seasonal dynamics and stem volume retrieval in boreal forests using JERS-1 backscatter," in *Remote Sensing for Agriculture, Ecosystems, and Hydrology Iv*, vol. 4879, M. Owe, G. D'Urso, and L. Toullos, Eds. Bellingham: Spie-Int Soc Optical Engineering, 2003, pp. 231–242.
- [18] M. Santoro, L. Eriksson, J. Askne, and C. Schmullius, "Assessment of stand-wise stem volume retrieval in boreal forest from JERS-1 L-band SAR backscatter," *International Journal of Remote Sensing*, vol. 27, no. 16, pp. 3425–3454, Aug. 2006.
- [19] S. Kumar, "Retrieval of forest parameters from Envisat ASAR data for biomass inventory in Dudhwa National Park, UP, India," *M. Sc., Indian Institute of Remote Sensing (IIRS) and International Institute for Geoinformation Science and Earth Observation (ITC)*, 2009.
- [20] X. Xu, A. Marino, and L. Li, "Biomass related parameter retrieving from quad-pol images based on Freeman-Durden decomposition," in *Geoscience and Remote Sensing Symposium (IGARSS), 2011 IEEE International*, 2011, pp. 405–408.
- [21] C. P. Tan, A. Marino, I. Woodhouse, S. Cloude, J. Suarez, and C. Edwards, "See the forests with different eyes," in *Geoscience and Remote Sensing Symposium (IGARSS), 2011 IEEE International*, 2011, pp. 1405–1408.
- [22] R. Touzi, W. M. Boerner, J. S. Lee, and E. Lueneburg, "A review of polarimetry in the context of synthetic aperture radar: concepts and information extraction," *Can. J. Remote Sens.*, vol. 30, no. 3, pp. 380–407, Jun. 2004.
- [23] J.-S. Lee and E. Pottier, *Polarimetric Radar Imaging: From Basics to Applications*, 1st ed. CRC Press, 2009.
- [24] J. S. Lee, D. L. Schuler, T. L. Ainsworth, and W.-M. Boerner, "Polarization orientation estimation and applications: a review," in *Geoscience and Remote Sensing Symposium, 2003. IGARSS '03. Proceedings. 2003 IEEE International*, 2003, vol. 1, pp. 428–430 vol.1.

- [25] J. S. Lee, E. Krogager, D. L. Schuler, T. L. Ainsworth, and W. M. Boerner, "On the estimation of polarization orientation angles induced from azimuth slopes using polarimetric SAR data," in *Geoscience and Remote Sensing Symposium, 2000. Proceedings. IGARSS 2000. IEEE 2000 International*, 2000, vol. 3, pp. 1310–1312 vol.3.
- [26] J. S. Lee, D. L. Schuler, T. L. Ainsworth, and W. M. Boerner, "POLARSAR data compensation for terrain azimuth slope variation," in *Geoscience and Remote Sensing Symposium, 1999. IGARSS '99 Proceedings. IEEE 1999 International*, 1999, vol. 5, pp. 2437–2439 vol.5.
- [27] D. L. Schuler, J.-S. Lee, and G. De Grandi, "Measurement of topography using polarimetric SAR images," *IEEE Transactions on Geoscience and Remote Sensing*, vol. 34, no. 5, pp. 1266–1277, Sep. 1996.
- [28] J.-S. Lee, T. L. Ainsworth, and K.-S. Chen, "The effect of orientation angle compensation on polarimetric target decompositions," presented at the Geoscience and Remote Sensing Symposium, 2009 IEEE International, IGARSS 2009, 2009, vol. 4, p. IV-849–IV-852.
- [29] S. R. Cloude and E. Pottier, "A review of target decomposition theorems in radar polarimetry," *IEEE Transactions on Geoscience and Remote Sensing*, vol. 34, no. 2, pp. 498–518, Mar. 1996.
- [30] S. R. Cloude, *Polarisation*. Oxford; New York: Oxford University Press, 2010.
- [31] S. R. Cloude, "Group theory and polarisation algebra," *Optik*, vol. 75, no. 1, pp. 26–36, 1986.
- [32] A. Freeman, "Fitting a Two-Component Scattering Model to Polarimetric SAR Data From Forests," *Geoscience and Remote Sensing, IEEE Transactions on*, vol. 45, no. 8, pp. 2583–2592, Aug. 2007.
- [33] Y. Yamaguchi, T. Moriyama, M. Ishido, and H. Yamada, "Four-component scattering model for polarimetric SAR image decomposition," *Geoscience and Remote Sensing, IEEE Transactions on*, vol. 43, no. 8, pp. 1699–1706, Aug. 2005.
- [34] A. Sato, Y. Yamaguchi, G. Singh, and S.-E. Park, "Four-Component Scattering Power Decomposition With Extended Volume Scattering Model," *IEEE Geoscience and Remote Sensing Letters*, vol. 9, no. 2, pp. 166–170, Mar. 2012.
- [35] "ECV T12 - BIOMASS : ESSENTIAL CLIMATE VARIABLES." GTOS, 2009.
- [36] G. Patenaude, R. Milne, and T. P. Dawson, "Synthesis of remote sensing approaches for forest carbon estimation: reporting to the Kyoto Protocol," *Environmental Science & Policy*, vol. 8, no. 2, pp. 161–178, Apr. 2005.
- [37] S. Ullah, Y. Si, M. Schlerf, A. K. Skidmore, M. Shafique, and I. A. Iqbal, "Estimation of grassland biomass and nitrogen using MERIS data," *International Journal of Applied Earth Observation and Geoinformation*, vol. 19, pp. 196–204, Oct. 2012.

- [38] L. R. Sarker and J. E. Nichol, "Improved forest biomass estimates using ALOS AVNIR-2 texture indices," *Remote Sensing of Environment*, vol. 115, no. 4, pp. 968–977, 2011.
- [39] J. E. Nichol and M. L. R. Sarker, "Improved Biomass Estimation Using the Texture Parameters of Two High-Resolution Optical Sensors," *IEEE Transactions on Geoscience and Remote Sensing*, vol. 49, no. 3, pp. 930–948, Mar. 2011.
- [40] M. Wulder, "Optical remote-sensing techniques for the assessment of forest inventory and biophysical parameters," *Progress in Physical Geography*, vol. 22, no. 4, pp. 449–476, Oct. 1998.
- [41] Å. Rosenqvist, A. Milne, R. Lucas, M. Imhoff, and C. Dobson, "A review of remote sensing technology in support of the Kyoto Protocol," *Environmental Science & Policy*, vol. 6, no. 5, pp. 441–455, Oct. 2003.
- [42] M. A. LEFSKY, W. B. COHEN, G. G. PARKER, and D. J. HARDING, "Lidar Remote Sensing for Ecosystem Studies," *BioScience*, vol. 52, no. 1, pp. 19–30, Jan. 2002.
- [43] J. B. Drake, R. O. Dubayah, D. B. Clark, R. G. Knox, J. B. Blair, M. A. Hofton, R. L. Chazdon, J. F. Weishampel, and S. Prince, "Estimation of tropical forest structural characteristics using large-footprint lidar," *Remote Sensing of Environment*, vol. 79, no. 2, pp. 305–319, 2002.
- [44] J. Boudreau, R. F. Nelson, H. A. Margolis, A. Beaudoin, L. Guindon, and D. S. Kimes, "Regional aboveground forest biomass using airborne and spaceborne LiDAR in Québec," *Remote Sensing of Environment*, vol. 112, no. 10, pp. 3876–3890, 2008.
- [45] K. Kronseder, U. Ballhorn, V. Böhm, and F. Siegert, "Above ground biomass estimation across forest types at different degradation levels in Central Kalimantan using LiDAR data," *International Journal of Applied Earth Observation and Geoinformation*, vol. 18, pp. 37–48, 2012.
- [46] T. Le Toan, A. Beaudoin, J. Riou, and D. Guyon, "Relating forest biomass to SAR data," *IEEE Transactions on Geoscience and Remote Sensing*, vol. 30, no. 2, pp. 403–411, Mar. 1992.
- [47] D. Lo Seen, A. Beaudoin, D. Girou, and T. Le Toan, *Tropical forest parameters retrieved from airborne multifrequency radar images*. New York: Ieee, 1998.
- [48] S. Paloscia, G. Macelloni, P. Pampaloni, and S. Sigismondi, "The potential of C- and L-band SAR in estimating vegetation biomass: the ERS-1 and JERS-1 experiments," *IEEE Transactions on Geoscience and Remote Sensing*, vol. 37, no. 4, pp. 2107–2110, Jul. 1999.
- [49] A. C. Morel, S. S. Saatchi, Y. Malhi, N. J. Berry, L. Banin, D. Burslem, R. Nilus, and R. C. Ong, "Estimating aboveground biomass in forest and oil palm plantation in Sabah, Malaysian Borneo using ALOS PALSAR data," *Forest Ecology and Management*, vol. 262, no. 9, pp. 1786–1798, Nov. 2011.

- [50] E. T. A. Mitchard, S. S. Saatchi, I. H. Woodhouse, G. Nangendo, N. S. Ribeiro, M. Williams, C. M. Ryan, S. L. Lewis, T. R. Feldpausch, and P. Meir, “Using satellite radar backscatter to predict above-ground woody biomass: A consistent relationship across four different African landscapes,” *Geophysical Research Letters*, vol. 36, no. 23, p. L23401, Dec. 2009.
- [51] C. C. Hsu, H. C. Han, R. T. Shin, J. A. Kong, A. Beaudoin, and T. Le Toan, “Radiative Transfer Theory For Polarimetric Remote Sensing of Pine Forest,” in *Geoscience and Remote Sensing Symposium, 1992. IGARSS '92. International, 1992*, vol. 2, pp. 1129–1131.
- [52] M. Burgin, D. Clewley, R. M. Lucas, and M. Moghaddam, “A Generalized Radar Backscattering Model Based on Wave Theory for Multilayer Multispecies Vegetation,” *IEEE Transactions on Geoscience and Remote Sensing*, vol. 49, no. 12, pp. 4832–4845, Dec. 2011.
- [53] M. Santoro, J. Askne, G. Smith, and J. E. . Fransson, “Stem volume retrieval in boreal forests from ERS-1/2 interferometry,” *Remote Sensing of Environment*, vol. 81, no. 1, pp. 19–35, Jul. 2002.
- [54] P. K. Mathur and N. Midha, “Mapping of National Parks and Wildlife Sanctuaries, Dudhwa Tiger Reserve, WII-NNRMS-MoEF Project,” Final Technical Report, Wildlife Institute of India, Dehradun, India, 2008.
- [55] U. Pandey, S. P. S. Kushwaha, T. S. Kachhwaha, P. Kunwar, and V. K. Dadhwal, “Potential of Envisat ASAR data for woody biomass assessment,” *Trop. Ecol.*, vol. 51, no. 1, pp. 117–124, SUM 2010.
- [56] A. Rosenqvist, M. Shimada, and M. Watanabe, “ALOS PALSAR: Technical outline and mission concepts,” in *4th International Symposium on Retrieval of Bio-and Geophysical Parameters from SAR Data for Land Applications*, 2004, pp. 1–7.
- [57] N. R. C. Government of Canada, “Tutorial: Radar Polarimetry | Earth Sciences,” 07-Feb-2007. [Online]. Available: <http://www.nrcan.gc.ca/earth-sciences/geography-boundary/remote-sensing/radar/1893>. [Accessed: 15-Aug-2012].
- [58] S. Kumar, “Retrieval of forest parameters from Envisat ASAR data for biomass inventory in Dudhwa National Park, UP, India,” *M. Sc., Indian Institute of Remote Sensing (IIRS) and International Institute for Geoinformation Science and Earth Observation (ITC)*, 2009.
- [59] Shashi Kumar, “Retrieval of forest parameters from ENVISAT ASAR data for biomass inventory in Dudhwa National Park, U.P., India,” ITC, 2009.
- [60] H. Wang and K. Ouchi, “A Simple Moment Method of Forest Biomass Estimation From Non-Gaussian Texture Information by High-Resolution Polarimetric SAR,” *IEEE Geoscience and Remote Sensing Letters*, vol. 7, no. 4, pp. 811–815, Oct. 2010.
- [61] M. L. Imhoff, “Radar backscatter and biomass saturation: ramifications for global biomass inventory,” *IEEE Transactions on Geoscience and Remote Sensing*, vol. 33, no. 2, pp. 511–518, Mar. 1995.

